Journal of the Mechanics and Physics of Solids 56 (2008) 3144–3166

Contents lists available at ScienceDirect

Journal of the Mechanics and Physics of Solids

journal homepage: www.elsevier.com/locate/jmps

Surface stress effects on the resonant properties of metal nanowires: The importance of finite deformation kinematics and the impact of the residual surface stress

Harold S. Park [a,*], Patrick A. Klein [b]

[a] Department of Mechanical Engineering, University of Colorado, Boulder, CO 80309, USA
[b] Franklin Templeton Investments, San Mateo, CA 94403, USA

ARTICLE INFO

Article history:
Received 5 January 2008
Received in revised form
6 August 2008
Accepted 13 August 2008

Keywords:
Nanowires
Resonant frequency
Surface stress
Surface Cauchy–Born
Finite elements

ABSTRACT

We utilize the recently developed surface Cauchy–Born model, which extends the standard Cauchy–Born theory to account for surface stresses due to undercoordinated surface atoms, to study the coupled influence of boundary conditions and surface stresses on the resonant properties of ⟨1 0 0⟩ gold nanowires with {1 0 0} surfaces. There are two major purposes to the present work. First, we quantify, for the first time, variations in the nanowire resonant frequencies due to surface stresses as compared to the corresponding bulk material which does not observe surface effects within a finite deformation framework depending on whether fixed/free or fixed/fixed boundary conditions are utilized. We find that while the resonant frequencies of fixed/fixed nanowires are elevated as compared to the corresponding bulk material, the resonant frequencies of fixed/free nanowires are reduced as a result of compressive strain caused by the surface stresses. Furthermore, we find that for a diverse range of nanowire geometries, the variation in resonant frequencies for both boundary conditions due to surface stresses is a geometric effect that is characterized by the nanowire aspect ratio. The present results are found to agree well with existing experimental data for both types of boundary conditions.

The second major goal of this work is to quantify, for the first time, how both the residual (strain-independent) and surface elastic (strain-dependent) parts of the surface stress impact the resonant frequencies of metal nanowires within the framework of nonlinear, finite deformation kinematics. We find that if finite deformation kinematics are considered, the strain-independent surface stress substantially alters the resonant frequencies of the nanowires; however, we also find that the strain-dependent surface stress has a significant effect, one that can be comparable to or even larger than the effect of the strain-independent surface stress depending on the boundary condition, in shifting the resonant frequencies of the nanowires as compared to the bulk material.

1. Introduction

Over the past decade, nanowires, both metallic and semiconducting, have drawn considerable interest from the scientific community (Xia et al., 2003; Lieber, 2003). The large interest in nanowires has largely been driven by their

* Corresponding author. Tel.: +1 303 492 7750; fax: +1 303 492 3498.
E-mail address: harold.park@colorado.edu (H.S. Park).

0022-5096/$ - see front matter © 2008 Elsevier Ltd. All rights reserved.
doi:10.1016/j.jmps.2008.08.003

remarkable physical properties, most of which emerge due to their small size and thus large surface area to volume (SAV) ratio. These properties range across the scientific disciplines, including unusual or enhanced optical (Canham, 1990; Barnes et al., 2003), electrical (Wiley et al., 2006; Rubio et al., 1996; Ohnishi et al., 1998), thermal (Li et al., 2003) and mechanical (Wong et al., 1997; Cuenot et al., 2004; Wu et al., 2005; Jing et al., 2006) properties.

Nanowires are also important as they will serve as the basic building blocks for future nanoelectromechanical systems (NEMS), which have been proposed for a multitude of cross-disciplinary applications, including chemical and biological sensing, force and pressure sensing, high frequency resonators, and many others (Cleland and Roukes, 1996; Huang et al., 2003; Craighead, 2000; Lavrik et al., 2004; Ekinci and Roukes, 2005; Ekinci, 2005). Because many of the proposed applications for nanowire-based NEMS, such as resonant mass sensing and high frequency oscillators (Craighead, 2000; Lavrik et al., 2004; Ekinci and Roukes, 2005) rely on the ability to control and tailor the nanowire resonant frequencies with a high degree of precision, it is critical to be able to predict and control variations in the nanowire resonant frequencies.

The potential of nanowires in future nanotechnologies has led to significant interest in experimental characterization of the size-dependent elastic properties of nanowires. The experimental techniques utilized have varied from time-resolved spectroscopy (Petrova et al., 2006) to AFM-induced bending (Wong et al., 1997; Wu et al., 2005; Heidelberg et al., 2006; Cuenot et al., 2004; Jing et al., 2006; Hoffmann et al., 2006; Chen et al., 2006; Namazu et al., 2000; Sundararajan et al., 2002) or resonance measurements (Verbridge et al., 2006, 2007; Cleland and Roukes, 1996; Husain et al., 2003; Nam et al., 2006; Dikin et al., 2003; Yang et al., 2001; Houston et al., 2002; Evoy et al., 2000). In general, resonance measurements to obtain the nanoscale elastic properties are predominant in the literature due to their relative simplicity as compared to bending and tensile experiments at the nanoscale due to the reduced amount of nanowire manipulation involved in resonance-based testing. The experimental results show significant scatter, with some predictions of enhanced elastic stiffness (Husain et al., 2003; Cuenot et al., 2004; Jing et al., 2006), some predicting reduced elastic stiffness (Petrova et al., 2006) with decreasing nanostructure size, and some predicting no change with respect to the bulk elastic stiffness (Wu et al., 2005; Heidelberg et al., 2006).

The difficulty in predicting the resonant properties of nanowires stems from the fact that they are characterized by a large SAV ratio; because of this, nanowires are subject to surface stresses (Cammarata, 1994; Haiss, 2001), which occur due to the fact that surface atoms have fewer bonding neighbors than do atoms that lie within the material bulk. Surface stresses have been predicted to cause many non-bulk phenomena in nanowires, including self-healing behavior and phase transformations (Diao et al., 2003; Park et al., 2005; Liang et al., 2005b), and non-bulk elastic properties (Zhou and Huang, 2004; Liang et al., 2005a; Dingreville et al., 2005; Cuenot et al., 2004; Jing et al., 2006; Shenoy, 2005).

The knowledge that surface effects are critical to understanding the mechanical behavior and properties of nanomaterials has motivated the development of enhanced continuum models, as standard continuum mechanics is length scale independent. Various analytic models have been developed to study the effects of surface stress on the resonant properties of nanobeams (Lu et al., 2005; Gurtin et al., 1976; Sader, 2001; McFarland et al., 2005), or more generally to capture the non-bulk mechanical properties of nanostructures (Gurtin and Murdoch, 1975; Miller and Shenoy, 2000; Shenoy, 2005; Sharma et al., 2003; Sun and Zhang, 2003; Dingreville et al., 2005; Wei et al., 2006; Wang et al., 2006; Tang et al., 2006; Lu et al., 2005; Gurtin et al., 1976; Sader, 2001; Huang et al., 2006; McFarland et al., 2005). Due to assumptions utilized to make the analyses tractable, the coupled effects of geometry, surface orientation and system size on the resonant properties of nanowires have not been quantified, nor have surface stress effects arising directly from atomistic principles been included in the analyses, which are generally in two-dimensions. The analyses also utilize overly simplistic pair-type atomic interactions to describe the surface physics, which tend to incorrectly predict a compressive surface stress for metals, whereas the surface stress for metals is almost always tensile. These errors indicate that quantitative analyses for real materials cannot be made using these approaches.

There are two major goals to the present work. The first is to quantify, for the first time, how surface stresses may be expected to alter the resonant frequencies for gold nanowires with a $\langle 1\,0\,0\rangle$ axial orientation and $\{1\,0\,0\}$ transverse surfaces considering both fixed/fixed and fixed/free boundary conditions as compared to the corresponding bulk material that does not observe nanoscale surface stress effects. These boundary conditions are ubiquitous in the study of NEMS, as most NEMS employ nanomaterials such as nanowires and nanotubes as the active beam element.

We obtain the resonant frequencies using the recently developed surface Cauchy–Born (SCB) model (Park et al., 2006; Park and Klein, 2007, 2008; Park, 2008a, b). The uniqueness of the SCB approach as compared to other analytical and theoretical (Gurtin and Murdoch, 1975; Miller and Shenoy, 2000; Shenoy, 2005; Sharma et al., 2003; Sun and Zhang, 2003; Dingreville et al., 2005; Wei et al., 2006; Wang et al., 2006; Tang et al., 2006; Lu et al., 2005; Gurtin et al., 1976; Sader, 2001; Huang et al., 2006; McFarland et al., 2005) surface elastic models is that it enables the solution of three-dimensional nanomechanical boundary value problems for displacements, stresses and strains in nanomaterials using standard nonlinear finite element (FE) techniques (Belytschko et al., 2002), with the nonlinear, finite deformation material constitutive response obtained directly from realistic interatomic potentials such as the embedded atom method (EAM) (Daw and Baskes, 1984). Furthermore, the usage of a standard FE formulation enables the consideration of arbitrary geometries and various materials once the SCB model has been developed.

Therefore, the resonant properties of the gold nanowires are determined by solving a standard FE eigenvalue problem for the resonant frequencies and associated mode shapes, with full accounting for surface stress effects through the FE stiffness matrix. The present analysis does not account for factors that are known to deleteriously impact the resonant properties of nanostructures, including clamping losses and thermoelastic damping (Ekinci et al., 2004; Cleland and

Roukes, 2002; Evoy et al., 1999; Ilic et al., 2004; Yasumura et al., 2000; Carr et al., 1999; Yang et al., 2000). We quantify the effects of surface stress on the fundamental resonant frequency as well as the higher order resonant frequencies corresponding to the deformation modes of second bending, twist and stretch for both fixed/free and fixed/fixed boundary conditions as functions of geometry, size and SAV ratio. We further compare the results to those obtained using the standard bulk Cauchy–Born (BCB) material, which does not account for surface stress effects, while making contact with existing experimental data on the resonant frequencies and elastic properties of metal nanowires.

The second major goal of the present work is to, for the first time within the framework of nonlinear, finite deformation kinematics, determine the effects of both the residual (strain-independent) and surface elastic (strain-dependent) parts of the surface stress on the resonant frequencies of metal nanowires. Since the work of Gurtin et al. (1976), researchers have consistently found that, within the confines of linear elastic continuum beam theory, the strain-independent surface stress has no effect on the resonant frequency of a cantilever beam. However, Huang and Sun (2007) have recently demonstrated that if nonlinear, finite deformation kinematics are considered, that the residual surface stress does in fact change the effective elastic properties of the nanostructure. We therefore quantify in this work the effects of the residual and surface elastic parts of the surface stress on the resonant properties of metal nanowires using a modified version of the SCB model in which the strain-dependent parts of the surface stress and surface stiffness are subtracted from the original, fully nonlinear SCB model.

2. SCB model

2.1. Overview

Details regarding the SCB model and its differences from the standard BCB model have been described in previous publications (Park et al., 2006; Park and Klein, 2007, 2008; Park, 2008a, b). Therefore, we briefly overview the main ideas of the SCB model here.

The BCB model is a hierarchical multiscale assumption that enables the calculation of continuum stress and moduli from atomistic principles (Tadmor et al., 1996). Because the BCB model does not consider surface effects, the SCB model was developed (Park et al., 2006; Park and Klein, 2007, 2008) such that the energy density of a material would include contributions not only from the bulk, but also the material surfaces thus leading to the incorporation of atomistic-based surface stress effects into standard continuum stress measures.

Both the BCB and SCB models are finite deformation constitutive models that explicitly represent the stretching and rotation of bonds undergoing large deformation through continuum mechanics-based kinematic quantities such as the deformation gradient $\mathbf{F}$, or the stretch tensor $\mathbf{C}=\mathbf{F}^{\mathrm{T}}\mathbf{F}$ (Belytschko et al., 2002). Under deformations which can be represented as homogeneous over the unit cell scale, the approximation exactly reproduces the response of the corresponding, fully atomistic representation of the crystal. The necessity for the finite deformation kinematics gains credence through recent work that has indicated that surface stresses can cause *nonlinearly elastic* compressive strains on the order of 1% or more in the nanowires (Park and Klein, 2007; Liang et al., 2005a). The finite deformation formulation utilized for the SCB model also enables the calculation of resonant frequencies of highly deformed nanostructures, which may be useful due to the large elastic deformations that nanowires can undergo prior to yield and subsequent failure and due to the numerous sensing applications that are envisioned utilizing nanowires as the sensing component (Ekinci and Roukes, 2005; Park, 2008a).

A schematic of the SCB decomposition of bulk/non-bulk atoms near a free surface is shown in Fig. 1; note that all atomic interactions involving bulk and non-bulk atoms are governed entirely by the range of the interatomic potential chosen, as would be in an atomistic simulation. Mathematically, the relationship between the continuum strain energy density and the total potential energy of the corresponding, defect-free atomistic system can be written as

$$\sum_{i}^{\text{natoms}} U_i(r)=\int_{\Omega_0^{\text{bulk}}}\Phi(\mathbf{C})\,\mathrm{d}\Omega+\int_{\Gamma_0^1}\gamma_{\Gamma_0^1}(\mathbf{C})\,\mathrm{d}\Gamma+\int_{\Gamma_0^2}\gamma_{\Gamma_0^2}(\mathbf{C})\,\mathrm{d}\Gamma+\int_{\Gamma_0^3}\gamma_{\Gamma_0^3}(\mathbf{C})\,\mathrm{d}\Gamma+\int_{\Gamma_0^4}\gamma_{\Gamma_0^4}(\mathbf{C})\,\mathrm{d}\Gamma, \tag{1}$$

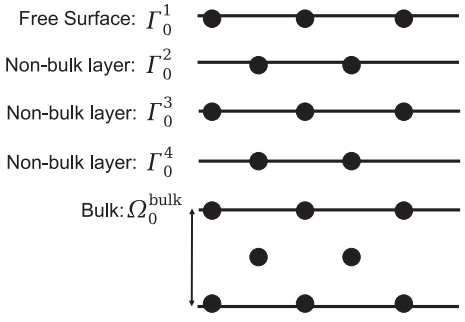

Fig. 1. Illustration of bulk and non-bulk layers of atoms in a ⟨1 0 0⟩/{1 0 0} FCC crystal interacting by an EAM potential.

where U_i is the potential energy for atom i, r is the interatomic distance, $\Phi(\mathbf{C})$ is the bulk strain energy density, Ω_0^{bulk} represents the volume of the body in which all atoms are fully coordinated, $\gamma_{\Gamma_0^a}(\mathbf{C})$ is the surface strain energy density of a representative atom in surface layer a and natoms is the total number of atoms in the system.

The bulk strain energy density $\Phi(\mathbf{C})$ in this work is obtained using EAM potentials (Daw and Baskes, 1984; Foiles et al., 1986), and takes the form

$$\Phi(\mathbf{C}) = \frac{1}{\Omega_0}(F_i(\bar{\rho}_i) + \phi_i), \tag{2}$$

$$\phi_i = \frac{1}{2}\sum_{j\neq i}^{\text{nbrv}_i} \phi_{ij}(r_{ij}(\mathbf{C})), \tag{3}$$

$$\bar{\rho}_i = \sum_{j\neq i}^{\text{nbrv}_i} \rho_j(r_{ij}(\mathbf{C})), \tag{4}$$

where nbrv_i are the number of bonds in the representative unit volume Ω_0 for atom i, F_i is the embedding function, ρ_j is the contribution to the electron density at atom i from atom j, ϕ_{ij} is a pair interaction function and r_{ij} is the distance between atoms i and j.

Analogous to the bulk energy density, the surface energy densities $\gamma(\mathbf{C})$ describe the energy per representative undeformed *area* of atoms at or near the surface of a homogeneously deforming crystal, and is also obtained using the same EAM potential as the bulk energy density. For FCC metals, choosing a surface unit cell that contains only one atom is sufficient to reproduce the structure of each surface layer. The surface unit cell possesses translational symmetry only in the plane of the surface, unlike the bulk unit cell which possesses translational symmetry in all directions. Thus, the surface energy density $\gamma_{\Gamma_0^a}(\mathbf{C})$ for a representative atom in a given surface layer Γ_0^a in Fig. 1 can be written as

$$\gamma_{\Gamma_0^a}(\mathbf{C}) = \frac{1}{\Gamma_0}(F_i(\bar{\rho}_i) + \phi_i), \tag{5}$$

$$\phi_i = \frac{1}{2}\sum_{j\neq i}^{\text{nb}_a} \phi_{ij}(r_{ij}(\mathbf{C})), \tag{6}$$

$$\bar{\rho}_i = \sum_{j\neq i}^{\text{nb}_a} \rho_j(r_{ij}(\mathbf{C})), \tag{7}$$

where nb_a are the number of bonds for an atom in surface layer a, and Γ_0 is the representative unit area occupied by a non-bulk atom lying at or near the free surface.

Once the bulk strain energy density is known, continuum stress measures such as the second Piola–Kirchoff stress $\mathbf{S}$ can be defined as

$$\mathbf{S} = 2\frac{\partial \Phi(\mathbf{C})}{\partial \mathbf{C}}, \tag{8}$$

while the material tangent modulus $\mathscr{C}$ is defined to be

$$\mathscr{C} = 2\frac{\partial \mathbf{S}}{\partial \mathbf{C}}. \tag{9}$$

Similarly, the surface stress on each surface layer Γ_0^a in Fig. 1 can be defined as

$$\tilde{\mathbf{S}}^{(a)}(\mathbf{C}) = 2\frac{\partial \gamma_{\Gamma_0^a}(\mathbf{C})}{\partial \mathbf{C}}, \tag{10}$$

while the surface tangent modulus $\tilde{\mathscr{C}}$ can be written as

$$\tilde{\mathscr{C}} = 2\frac{\partial \tilde{\mathbf{S}}}{\partial \mathbf{C}}. \tag{11}$$

The SCB model thus uses the surface unit cells based on the surface energies $\gamma(\mathbf{C})$ to capture the undercoordination of atoms in the surface layers. Because the surface unit cells are undercoordinated, they are not at a minimum energy at the same atomistic spacing as bulk atoms, which results in the existence of surface stresses in Eq. (10) through differentiation of the surface energies $\gamma(\mathbf{C})$. It is critical to emphasize again that both the surface stress in Eq. (10) and the surface tangent modulus in Eq. (11) are quantities based upon finite deformation kinematics that are functions of strain through the stretch tensor $\mathbf{C}$.

We also discuss here differences between the current formulation for surface stress and surface energy, and the traditional thermodynamic definition of surface stress (see for example Cammarata, 1994; Shenoy, 2005):

$$\tau = \tau_0 + \mathbf{C}_0\boldsymbol{\varepsilon}, \tag{12}$$

where τ is the surface stress, τ_0 is the residual (strain-independent) portion of the surface stress, $\mathbf{C}_0\boldsymbol{\varepsilon}$ is the surface-elastic (strain-dependent) part of the surface stress, and where $\mathbf{C}_0$ is the (constant) surface elastic stiffness. We will return to this definition of surface stress later when investigating the effects of the strain-independent part of the surface stress on the nanowire resonant frequencies.

The thermodynamic interpretation of both the surface stress τ in Eq. (12) and that of the surface energy $\gamma_{\Gamma_0^a}(\mathbf{C})$ in Eq. (5) is that of an excess quantity, i.e. a measure of the difference as compared to the equivalent bulk quantity. The surface energy $\gamma_{\Gamma_0^a}(\mathbf{C})$ in Eq. (5) differs from the conventional definition in that it does not represent the excess, or difference in surface energy as compared to a typical bulk atom; instead, it represents the actual potential energy of an atom lying in surface layer a.

Furthermore, the definition of surface stress utilized in the present work in Eq. (10) differs from Eq. (12) in that the surface energy is directly differentiated in the present work to obtain the surface stress in Eq. (10). This choice can be understood by analyzing the energy balance in Eq. (1). Because Eq. (1) represents the total energy of the nanostructure as decomposed into bulk and surface contributions, minimization of the energy leads directly to a force balance (Park et al., 2006; Huang and Wang, 2006), which carries the clear physical meaning that at equilibrium, the bulk forces will balance the surface forces that originate from the surface stress. Furthermore, starting from the energy balance in Eq. (1) is extremely favorable for nonlinear FE implementation; the full details of the FE equations are found in Park et al. (2006). We note in closing that an extensive analysis of the SCB model in calculating the minimum energy configurations of gold nanowires as compared to benchmark atomistic calculations can be found in Park and Klein (2007).

2.2. FE eigenvalue problem for nanowire resonant frequencies

The equation describing the eigenvalue problem for continuum elastodynamics is written as

$$(\mathbf{K} - \omega^2\mathbf{M})\mathbf{u} = 0, \tag{13}$$

where $\mathbf{M}$ is the mass matrix and $\mathbf{K}$ is the stiffness matrix of the discretized FE equations; the solution of the eigenvalue problem described in Eq. (13) gives the resonant frequencies f, where $f = \omega/2\pi$ and the corresponding mode shapes $\mathbf{u}$. We note that the stiffness matrix $\mathbf{K}$ contains the effects of both material and geometric nonlinearities through a consistent linearization about the finitely deformed configuration (Belytschko et al., 2002).

As detailed in Park and Klein (2007), once the total energy is obtained by subtracting from Eq. (1) the work due to external loads, the FE equilibrium equations can be obtained by approximating the displacement field using standard FE interpolation functions (Belytschko et al., 2002) and taking the first variation of the total energy.

We emphasize that the addition of the surface energy terms in Eq. (1) leads naturally to the incorporation of the surface stresses in the FE stiffness matrix $\mathbf{K}$, which then leads to the dependence of the resonant frequencies f on the surface stresses. The eigenvalue problem was solved using the Sandia-developed package Trilinos, which was incorporated into the simulation code Tahoe.

3. Numerical examples

All numerical examples were performed on three-dimensional, single crystal gold nanowires that have a cross-section of width a and length h as illustrated in Fig. 2. Three different parametric studies are conducted in this work, which consider nanowires with constant cross-sectional area (CSA), constant length and constant SAV; the geometries are summarized in Table 1.

All wires had a $\langle 1\,0\,0\rangle$ longitudinal orientation with $\{1\,0\,0\}$ transverse surfaces, and had either fixed/free (cantilevered) boundary conditions, where the left $(-x)$ surface of the wire was fixed while the right $(+x)$ surface of the wire was free, or fixed/fixed boundary conditions, where both the left $(-x)$ and right $(+x)$ surfaces of the wire were fixed. All FE simulations were performed using the stated boundary conditions without external loading, and utilized regular meshes of 8-node hexahedral elements. The SCB bulk and surface energy densities in Eqs. (2) and (5) were calculated using EAM interatomic potentials, with gold being the material for all problems using the parameters of Foiles et al. (1986). In the present work, the bulk FE stresses were calculated using Eq. (8) and the surface FE stresses were found using Eq. (10).

We note also that the nanowire cross-sections considered in this work are sufficiently large such that the nanowire surfaces do not reconstruct or reorient to a lower energy orientation; it is well-established (Kondo et al., 1999; Hasmy and Medina, 2002) that gold $\{1\,0\,0\}$ surfaces will reorient to lower energy $\{1\,1\,1\}$ surfaces only if the thin film or nanowire

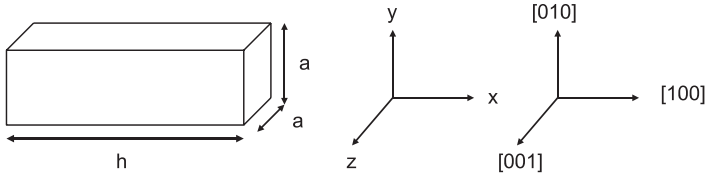

Fig. 2. Nanowire geometry considered for numerical examples.

Table 1
Summary of geometries considered: constant surface area to volume ratio (SAV), constant length, and constant cross-sectional area (CSA)

Constant SAV	Constant length	Constant CSA
64 × 16 × 16	232 × 9.7 × 9.7	64 × 16 × 16
110 × 15.2 × 15.2	232 × 11.6 × 11.6	128 × 16 × 16
170 × 14.9 × 14.9	232 × 15.95 × 15.95	256 × 16 × 16
230 × 14.7 × 14.7	232 × 23.2 × 23.2	384 × 16 × 16
290 × 14.5 × 14.5		

All dimensions are in nm.

thickness is less than about 2 nm. Thus, the {1 0 0} nanowire surfaces in this work undergo only nonlinear elastic deformations.

Regardless of boundary condition, the nanowires are initially out of equilibrium due to the presence of the surface stresses. For fixed/free nanowires, the free end undergoes a compressive relaxation strain to find an energy minimizing configuration under the influence of surface stresses; previous work (Park and Klein, 2007) illustrated the accuracy of the SCB model in predicting energy minimizing configurations of the nanowires due to surface stresses. Fixed/fixed nanowires, on the other hand, are constrained such that the nanowire free surfaces are unable to contract due to the boundary conditions. Therefore, fixed/fixed nanowires exist in a state of tension, as they are unable to contract despite the presence of the surface stresses. For both boundary conditions, the minimum energy configuration was obtained while accounting for the surface stresses.

The fixed/fixed boundary conditions utilized in this work represent nanowires that are fabricated through a top-down process of etching or lifting-off of a metal film on a semiconducting substrate (Davis and Boisen, 2005; Li et al., 2003, 2007) as is commonly done in experimental studies of NEMS-based nanowire resonance. Experimentally, the residual tension in the fixed/fixed nanowires would occur due to surface stress effects on the nanowires that are etched in a fixed configuration, and are therefore unable to contract axially to relieve the tensile surface stresses.

At that point, the eigenvalue problem described in Eq. (13) is solved using the FE stiffness matrix from the equilibrated (deformed) nanowire configuration to find the resonant frequencies. Resonant frequencies were also found using the standard BCB model (without surface stresses) on the same geometries for comparison. For all resonant frequencies reported in this work, the fundamental, or lowest mode frequencies corresponded to a standard bending mode of deformation.

For each nanowire geometry, we plot the resonant frequencies in two ways. First, we plot the normalized resonant frequency f_{scb}/f_{bcb} versus the aspect ratio h/a. Second, we plot the normalized resonant frequency f_{scb}/f_{bcb} versus the SAV ratio to quantify the resonant frequency variation that the surface stresses cause. Finally, we compare the results for the fixed/free nanowires to those of the fixed/fixed nanowires to ascertain the effects of boundary conditions and surface stresses on the predicted resonant frequencies.

3.1. Constant CSA

For the first set of simulations, nanowires with constant square cross-section of width $a = 16$ nm and increasing length h were considered; the lengths h considered ranged between four and 24 times a, resulting in FE meshes that contained between 5000 and 29 000 nodes.

To validate the accuracy of the calculations for the bulk material, we compare in Tables 2 and 3 the BCB and SCB resonant frequencies to those obtained using the well-known analytic solution for the fundamental resonant frequency for both fixed/free (cantilevered) and fixed/fixed beams (Weaver et al., 1990). For the fixed/free beam:

$$f_0 = \frac{B_0^2}{2\pi h^2}\sqrt{\frac{EI}{\rho A}}, \tag{14}$$

where $B_0 = 1.875$ for the fundamental resonant mode and E is the modulus in the ⟨1 0 0⟩ direction, which can be found to be 35 GPa (Foiles et al., 1986). The BCB resonant frequencies compare quite well to those predicted by the analytic formula, with increasing accuracy for increasing aspect ratio h/a, as would be expected from beam theory. We note that the SCB resonant frequencies become smaller than the bulk resonant frequencies when the aspect ratio $h/a > 8$; reasons for this trend, which will be observed in all parametric studies, will be discussed later.

For the fixed/fixed beam, the analytic solution is given as (Weaver et al., 1990)

$$f_0 = \frac{i^2\pi}{2h^2}\sqrt{\frac{EI}{\rho A}}, \tag{15}$$

where i is a mode shape factor, which is about 1.5 for the fundamental bending mode of fixed/fixed beams with zero displacement and zero slope boundary conditions (Verbridge et al., 2006; Weaver et al., 1990). Table 3 shows that the bulk

Table 2
Summary of constant CSA nanowire fundamental resonant frequencies for fixed/free boundary conditions as computed from: (1) the analytic solution given by Eq. (14), (2) bulk Cauchy–Born (BCB), and (3) surface Cauchy–Born (SCB)

Geometry	Eq. (14)	BCB	SCB
$64 \times 16 \times 16$	873	917	922
$128 \times 16 \times 16$	218	226	225
$256 \times 16 \times 16$	55	56	54
$384 \times 16 \times 16$	24	25	23

All frequencies are in MHz, the nanowire dimensions are in nm.

Table 3
Summary of constant CSA nanowire fundamental resonant frequencies for fixed/fixed boundary conditions as computed from: (1) the analytic solution given by Eq. (15), (2) bulk Cauchy–Born (BCB), and (3) surface Cauchy–Born (SCB)

Geometry	Eq. (15)	BCB	SCB
$64 \times 16 \times 16$	5370	5450	5730
$128 \times 16 \times 16$	1340	1430	1560
$256 \times 16 \times 16$	336	358	440
$384 \times 16 \times 16$	153	159	226

All frequencies are in MHz, the nanowire geometry is in nm.

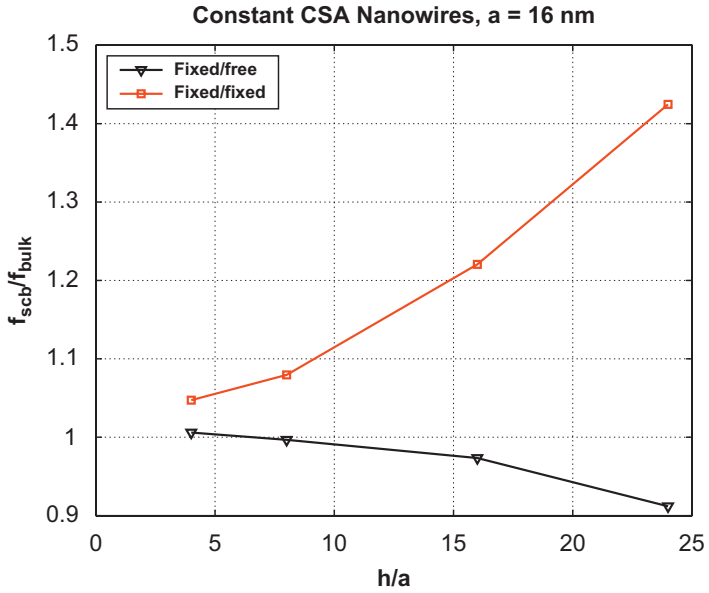

Fig. 3. Variation in fundamental resonant frequency for fixed/free and fixed/fixed constant cross-sectional area nanowires as a function of nanowire aspect ratio h/a.

CB and analytic frequencies agree nicely, while the SCB resonant frequencies are consistently higher; the reasons for this will be discussed in detail below.

Fig. 3 shows the resonant frequencies for both the fixed/fixed and fixed/free cases plotted as a function of the aspect ratio h/a. As can be seen, the calculated resonant frequencies vary greatly depending on the boundary condition. For small aspect ratios, both boundary conditions give resonant frequencies close to the bulk value. However, as the aspect ratio h/a increases, the fixed/free resonant frequencies decrease relative to the bulk value, while the fixed/fixed resonant frequencies increase relative to the bulk value. For the fixed/free case calculated in this work, the resonant frequency is reduced to nearly 90% of the bulk value when the aspect ratio reaches $h/a = 24$, while the resonant frequency for fixed/fixed nanowires increase to more than 140% of the bulk value when $h/a = 24$.

The results can also be analyzed with respect to the SAV ratio, as seen in Fig. 4. We note that in this case, increasing the length while keeping the CSA constant leads to a decrease in SAV ratio. Again, the boundary conditions impact the trends with SAV ratio; while the fixed/fixed nanowires show a decrease in resonant frequency with increasing SAV ratio, the opposite is observed for the fixed/free nanowires.

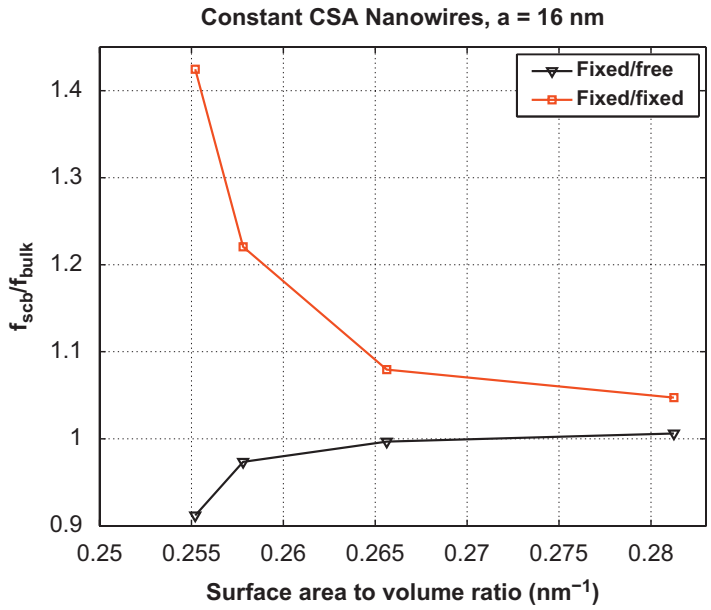

Fig. 4. Variation in fundamental resonant frequency for fixed/free and fixed/fixed constant cross-sectional area nanowires as a function of surface area to volume ratio.

3.2. Constant length

Simulations were also performed keeping the length of the nanowire fixed at $h = 232$ nm, while increasing the CSA. Aspect ratios of $h/a = 10$–24 were studied to quantify the variation in resonant frequencies for the two boundary conditions; the resulting FE meshes ranged in size from about 16 000 to 46 000 nodes.

The normalized resonant frequencies are plotted versus aspect ratio h/a in Fig. 5. Again, the fixed/fixed nanowires show a marked increase in resonant frequency with increasing h/a, while the fixed/free nanowires show a marked decrease in resonant frequency with h/a. For the smallest nanowires considered in this work, with a transverse dimension of 9.7 nm, the fixed/free resonant frequency is only 90% of the bulk value, while the fixed/fixed resonant frequency is more than 160% of the bulk value. In all cases, the fixed/free resonant frequencies are below the bulk value.

An interesting result is obtained when the resonant frequencies for the constant length geometry are plotted against SAV ratio in Fig. 6. Unlike the constant CSA resonant frequencies shown in Fig. 4, the fixed/free resonant frequencies *decrease* with increasing SAV ratio, while the fixed/fixed resonant frequencies *increase* with increasing SAV ratio.

3.3. Constant SAV ratio

To draw general conclusions about the impact of SAV ratio on the nanowire resonant frequencies, we calculate the resonant frequencies of nanowires that have the same SAV ratio ($0.28\ nm^{-1}$), but different square cross-sections of length a and longitudinal length h; a ranged from 14.5 to 16 nm, while h ranged from 64 to 290 nm, leading to FE mesh sizes ranging from about 5000 to 25 000 nodes.

The results for the constant SAV ratio nanowires are shown in Fig. 7; in this case, because the SAV ratio is constant, we plot the resonant frequencies for both boundary conditions only with respect to the aspect ratio h/a.

Fig. 7 clearly shows that the resonant frequency does not remain constant if the SAV ratio remains constant, for either fixed/free or fixed/fixed boundary conditions. In fact, the results strongly mirror those presented earlier in Fig. 3 for the constant CSA nanowires, and thus indicate that the nanowire aspect ratio h/a is a much more reliable tool to controlling, predicting and tailoring the resonant frequencies of nanowires than is the SAV ratio. This fact will be discussed later in this work.

3.4. Higher order modes

In addition to analyzing boundary condition and surface stress effects on the fundamental resonant frequencies of gold nanowires, we also now analyze their effects on the higher order resonant frequencies corresponding to the modes of second bending, twist and stretch.

We first plot the higher order mode resonant frequencies normalized by the corresponding bulk values of each mode for the two boundary conditions and for the constant CSA nanowires. The fixed/fixed higher order modes are plotted in Fig. 8, while the fixed/free higher order modes are plotted in Fig. 9. In both cases, the largest variation occurs in the second

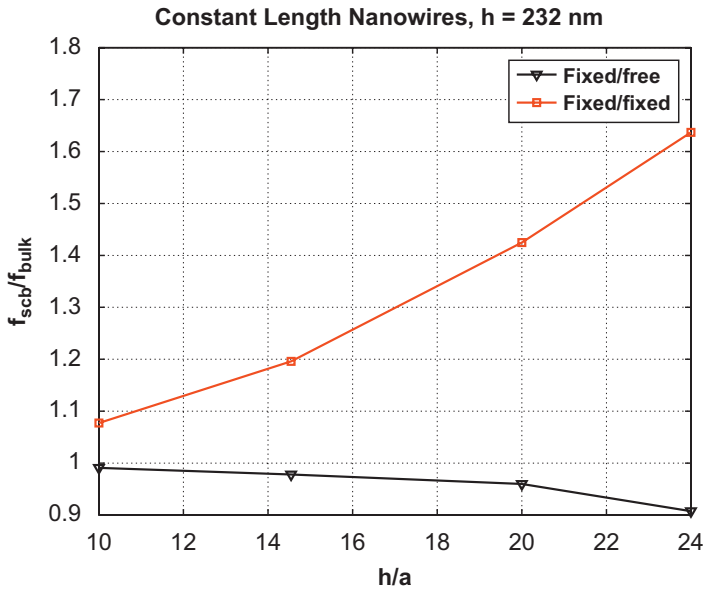

Fig. 5. Variation in fundamental resonant frequency for fixed/free and fixed/fixed constant length nanowires as a function of nanowire aspect ratio h/a.

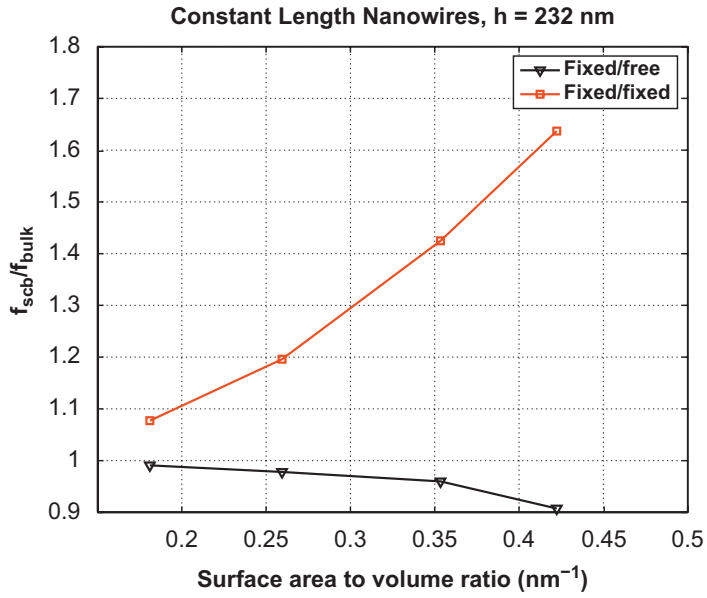

Fig. 6. Variation in fundamental resonant frequency for fixed/free and fixed/fixed constant length nanowires as a function of surface area to volume ratio.

bending mode resonant frequency, which increases with h/a for the fixed/fixed case similar to the fundamental mode resonant frequency, and decreases with h/a for the fixed/free case, again similar to the fundamental mode resonant frequency. In contrast, the twist and stretch frequencies show little variation with increasing aspect ratio h/a.

We also plot in Figs. 10 and 11 the variation in the higher mode resonant frequencies by normalizing each mode resonant frequency for both the BCB and SCB calculations by the first (fundamental) bending mode resonant frequency ($f^{scb}_{stretch}/f^{scb}_{bend1}$, $f^{bulk}_{stretch}/f^{bulk}_{bend1}$, etc.), to quantify how surface stresses cause the higher mode (second bending, stretch, twist) resonant frequencies to either increase or decrease relative to the fundamental bending resonant frequency.

Figs. 10 and 11 illustrate two points: first, how the higher mode (second bending, twist, stretch) resonant frequencies change with respect to the fundamental resonant frequency with increasing h/a, and second, how surface stresses alter the changes as compared to the BCB material. These figures again illustrate the effects of boundary conditions and surface stresses on the resonant frequencies. For example, in the fixed/fixed case in Fig. 10, all higher mode resonant frequencies decrease due to the surface stresses, with the effects being particularly dramatic for the stretch and twist modes; the $f_{stretch}/f_{bend1}$ ratio including surface stresses is only 71% of the equivalent bulk ratio when $h/a = 24$, while the twist differential is nearly identical. Similarly, the f_{bend2}/f_{bend1} ratio including surface stresses is about 87% of the bulk ratio when $h/a = 24$.

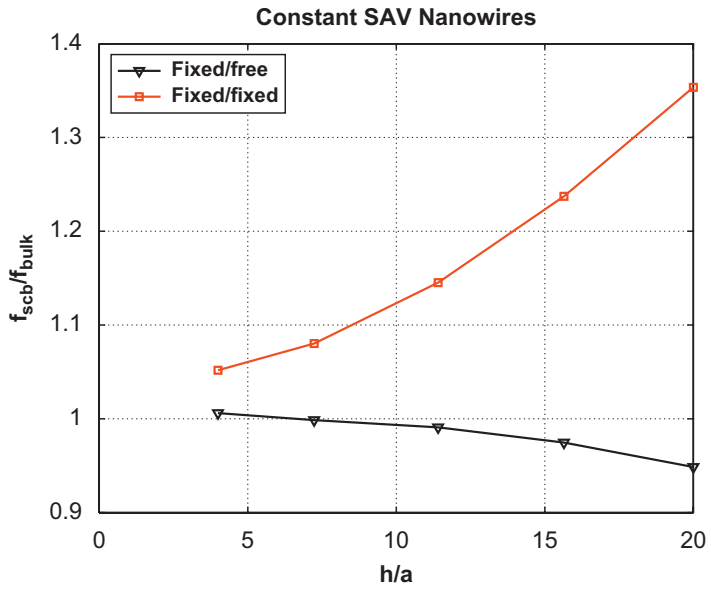

Fig. 7. Variation in fundamental resonant frequency for fixed/free and fixed/fixed constant surface area to volume ratio nanowires as a function of nanowire aspect ratio h/a.

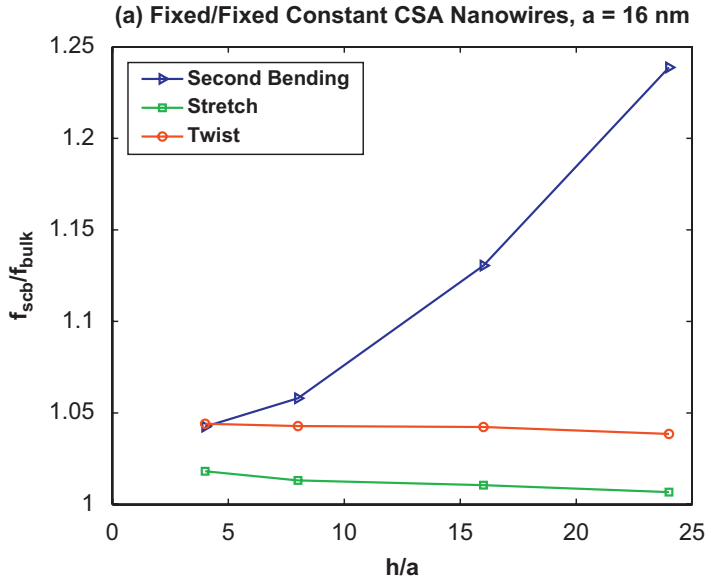

Fig. 8. Surface stress effects on higher mode resonant frequencies for fixed/fixed nanowires with constant cross-sectional area.

The trends for the fixed/free nanowires are completely different, as shown in Fig. 11. There, all higher mode resonant frequencies increase due to the surface stresses relative to the fundamental resonant frequency. The $f_{\text{stretch}}/f_{\text{bend1}}$ ratio including surface stresses is 108% of the equivalent bulk ratio when $h/a = 24$, while $f_{\text{twist}}/f_{\text{bend1}}$ is 116% of the equivalent bulk ratio. Similarly, the $f_{\text{bend2}}/f_{\text{bend1}}$ ratio including surface stresses is about 109% of the bulk ratio when $h/a = 24$.

4. Discussion, analysis and comparison to existing theoretical and experimental studies

4.1. Fixed/fixed nanowires

We now turn our attention to the fact that the resonant frequencies of fixed/fixed nanowires due to surface stresses as predicted using the SCB model are consistently larger than the resonant frequencies of the corresponding bulk material. Experimental measurements of the elastic properties of metal nanowires have generally focused upon using the atomic force microscope (AFM) to calculate the elastic properties through bending related techniques (Wu et al., 2005; Heidelberg

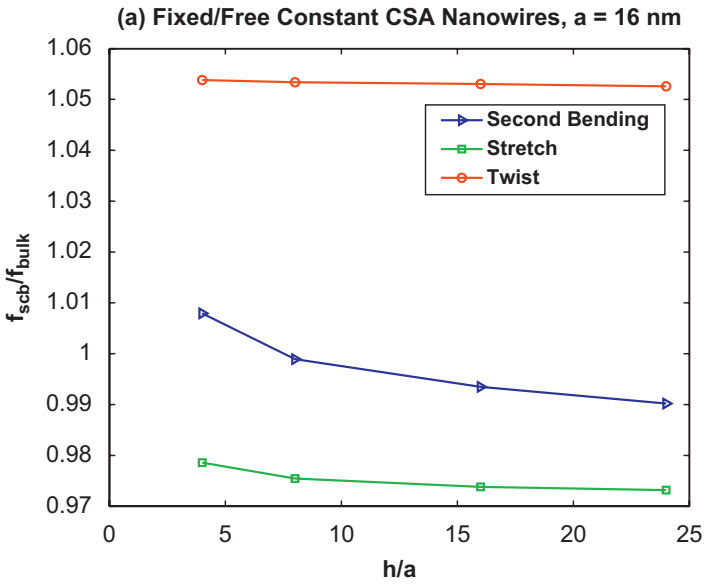

Fig. 9. Surface stress effects on higher mode resonant frequencies for fixed/free nanowires with constant cross-sectional area.

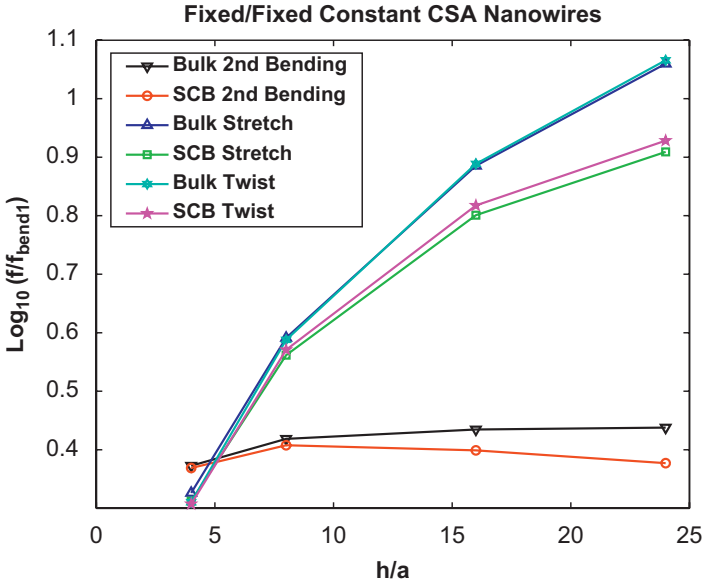

Fig. 10. Surface stress effects on higher mode resonant frequencies relative to the fundamental bending frequency for fixed/free nanowires with constant cross-sectional area.

et al., 2006; Jing et al., 2006). Alternatively, some researchers have utilized resonance-based measurements to extract the elastic properties. One such study was performed by Cuenot et al. (2004), who utilized electrostatic resonant-contact AFM to determine Young's modulus of silver and lead nanowires by first calculating the resonant frequencies. The nanowires analyzed in that work had fixed/fixed boundary conditions, while the diameters ranged from about 50 to 200 nm. The major finding of the Cuenot et al. work is that the nanowire Young's modulus (and therefore the resonant frequency) increases with respect to the bulk value with a reduction in CSA. Similar results were obtained by Jing et al. (2006), who utilized an AFM to perform three-point bend tests to extract the elastic properties of fixed/fixed silver nanowires. For nanowires with diameters ranging from 20 to 140 nm, similar results to those of Cuenot et al. were obtained, i.e. an increasing modulus with decreasing size.

Due to the existence of an analytic solution that was derived by Cuenot et al. (2004) to model the observed increase in nanowire Young's modulus with decreasing size for the fixed/fixed boundary conditions, we compare results obtained in the present work with their analytic solution. From the work of Cuenot et al. (2004), the analytic solution is

$$E_{\text{scb}} = E_{\text{bulk}} + \frac{8}{5}(1-\nu)\gamma\frac{h^2}{D^3}, \tag{16}$$

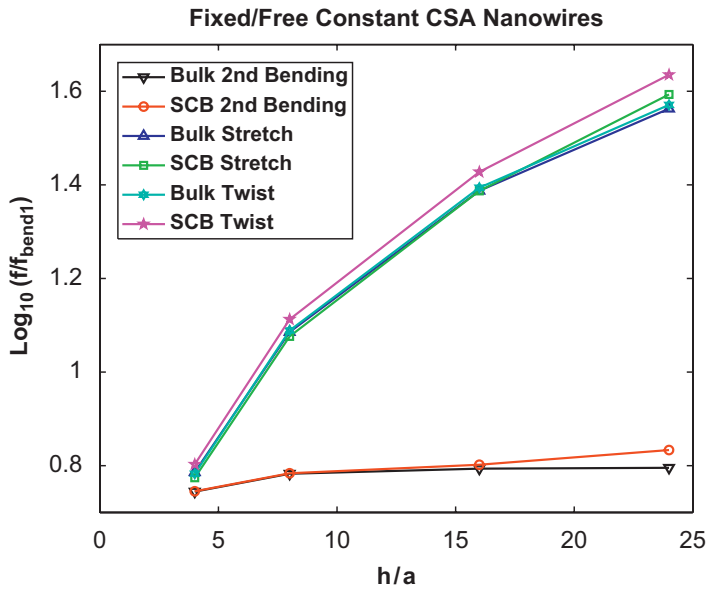

Fig. 11. Surface stress effects on higher mode resonant frequencies relative to the fundamental bending frequency for fixed/free nanowires with constant cross-sectional area.

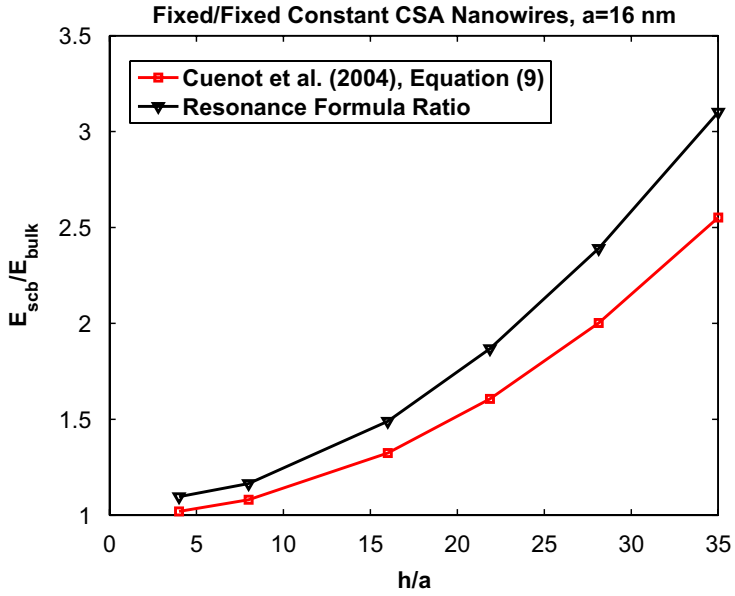

Fig. 12. E_{scb}/E_{bulk} as a function of aspect ratio h/a due to surface stress effects for fixed/fixed constant CSA nanowires.

where h is the nanowire length, E_{scb} is the apparent Young's modulus taking surface effects into account, E_{bulk} is the bulk Young's modulus, D is the nanowire diameter, γ is the surface energy and v is Poisson's ratio. We note that Eq. (16) implies that the modulus of the nanowires will change both as functions of the length, cross-sectional diameter, and therefore the aspect ratio. Here, the relaxed $\{1\,0\,0\}$ surface energy $\gamma = 0.914\,\mathrm{J/m^2}$ for the Foiles et al. (1986) potential was utilized, while the bulk Poisson's ratio of 0.44 for gold was utilized. We also note that in the Cuenot et al. (2004) work, the analytic relation in Eq. (16) was not actually utilized to compare against the experimentally obtained results.

Fig. 12 thus shows the E_{scb}/E_{bulk} ratio for the present work, which is obtained by substituting the numerically obtained resonant frequencies for both the SCB and BCB cases into Eq. (15) to solve for the SCB and BCB Young's moduli. We utilize the standard continuum beam theory equation in Eq. (15) to solve for the SCB Young's modulus due to the fact that the analytic solution given in Eq. (16) is also based upon continuum beam theory.

As can be seen, the modulus ratio obtained through the present work agrees well with the analytic solution of Cuenot et al. (2004) for the aspect ratios considered in this work, and illustrates that the expected length dependence of the nanowire Young's modulus is captured in the present work. The present results are not expected to agree exactly with the analytic solution in Eq. (16) for multiple reasons; the major reasons include the fact that metal nanowires typically form

oxide layers on the surface (Jing et al., 2006; Cuenot et al., 2004), and also because the SCB resonant frequencies were calculated using finite deformation kinematics, where the stiffness of the nanowire changes due to deformation induced by surface stresses. In contrast, the Cuenot et al. (2004) beam theory solution is based upon linear elasticity, and therefore constant material properties for both the bulk and surface components.

Despite these uncertainties, the general trend in Fig. 12 of increasing nanowire Young's modulus with increasing aspect ratio for fixed/fixed boundary conditions is correctly predicted using the SCB model. More importantly, Cuenot et al. (2004) experimentally observed an increase in apparent Young's modulus with decreasing size for fixed/fixed silver nanowires; the same trend is predicted in the present work for gold, and is explained naturally by understanding that the fixed/fixed nanowires exist in a state of tensile stress due to the fixed/fixed boundary conditions, which prevent surface stresses from contracting the nanowires.

We also compare our results with those obtained from Husain et al. (2003); we make this comparison due to the fact that they also studied the resonant properties of a fixed/fixed FCC nanowire, in this case platinum. To compare with their larger nanowires (cross-section of 43 nm, length of 1300 nm), we created gold nanowires of the same dimensions, and calculated the resonant frequency using the SCB model. The Husain et al. (2003) work found a resonant frequency for their fixed/fixed platinum nanowire of about 105 MHz, which exceeds the predicted value of 69 MHz as calculated using Eq. (15), with the experimentally measured resonant frequency being 1.5 times larger than the predicted resonant frequency.

For gold, the predicted resonant frequency using Eq. (15) should be about 35 MHz; the SCB calculations predicted a resonant frequency of 47.5 MHz, thus leading to the SCB results being about 1.4 times larger than that expected using Eq. (15). In the Husain et al. (2003) work, thermal effects due to mismatch between the nanowire and the substrate were cited as being a likely cause for placing their platinum nanowire under tension. The present results indicate that surface stress effects are likely to have played a role in elevating the experimentally observed resonant frequencies above those predicted using bulk continuum measures.

We also discuss the experiments of Verbridge et al. (2006), who studied the effect of applied tensile stress on the resonant frequencies of fixed/fixed SiN nanowires. This study is of relevance as it is one of the few to study the effects of tensile stresses on the resonant frequencies of nanowires, and thus is analogous to our situation where surface stresses cause a tensile stress within the gold nanowires.

A key finding of that work was the fact that the resonant frequency was found to vary linearly with the inverse of length; as shown in Verbridge et al. (2006), the resonant frequency of a beam under high tensile stress can be written as

$$f = \frac{i}{2h}\sqrt{\frac{S}{\rho A}}, \tag{17}$$

where S is the force in the beam. Interestingly, as can be seen in Fig. 13, both the SCB and BCB resonant frequencies scale linearly with $1/h^2$, instead of $1/h$. The bulk dependence on $1/h^2$ is not surprising considering the $1/h^2$ dependence of the analytic solution given in Eq. (15).

However, the same dependence of the SCB resonant frequencies is interesting, and implies that the surface stresses, and the nonlinear elastic deformation they cause in the nanowire, may be responsible for the variation from the behavior observed experimentally in the larger (100 nm) SiN nanowires. We also note that the different surface stresses of metallic (generally tensile Wan et al., 1999) and semiconductor (sometimes compressive Balamane et al., 1992) surfaces may also help to explain the observed differences. Finally, for the nanowires considered in that work, it is likely that the 100 nm cross-section is too large for surface stresses to have a significant effect on the mechanical properties, and thus the measured resonant frequencies.

4.2. Fixed/free nanowires

The large disparity in the calculated resonant frequencies between the fixed/free and fixed/fixed cases indicates that the nanowire stiffness and state of stress is strongly dependent on the boundary conditions. As previously discussed, the fixed/fixed boundary conditions prevent the nanowires from relaxing axially, as would occur due to surface stresses if one of the ends were free (Diao et al., 2003; Park et al., 2005; Liang et al., 2005b). Thus, the fixed/fixed nanowires exist in a state of tension, which elevates their resonant frequencies as compared to the unstrained fixed/fixed bulk material.

However, when fixed/free boundary conditions are utilized, the free end of the nanowire is able to contract axially in response to the tensile surface stresses, thereby reducing their transverse surface area and finding a minimum energy configuration. The prediction of the fixed/free resonant frequencies is therefore dependent on obtaining the correct stiffness of the nanowires after the surface-stress-driven relaxation has occurred; previous work (Park and Klein, 2007) indicated the ability of the SCB model to predict the correct relaxation strain due to surface stresses.

Fig. 14 illustrates one of the key findings of this work. In Fig. 14, we plot the variation in the fixed/free nanowire resonant frequencies due to surface stresses for all three geometries considered in this work (constant CSA, constant length, constant SAV ratio) versus the nanowire aspect ratio h/a. As can be seen, for the diverse geometries we have considered, the variations in resonant frequency due to surface stresses are quite similar as a function of h/a, indicating that the resonant frequency variation is purely geometric in nature.

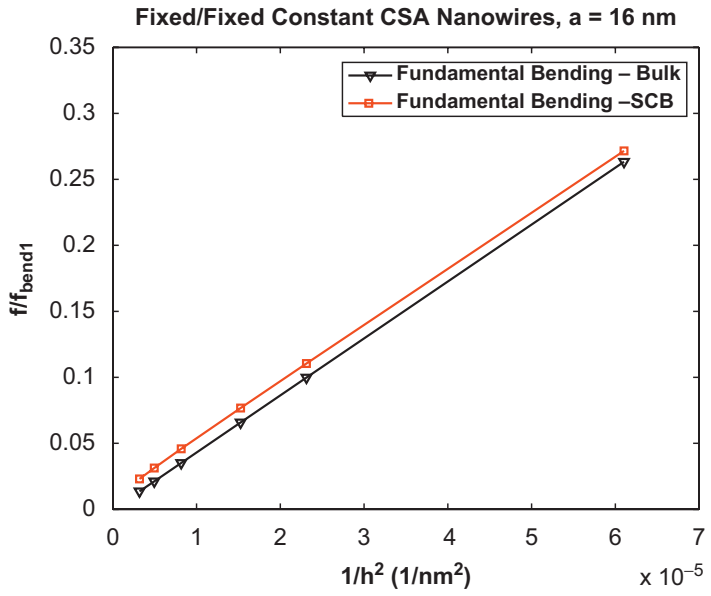

Fig. 13. Linear variation of both SCB and bulk CB resonant frequencies for constant CSA nanowires as a function of $1/h^2$.

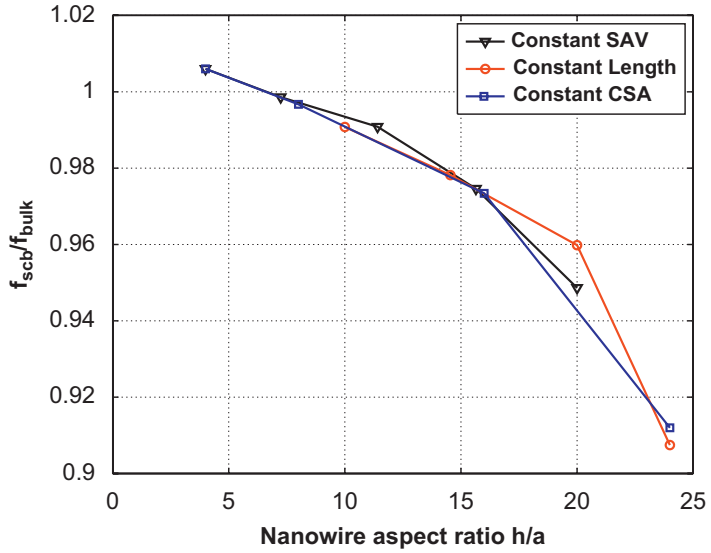

Fig. 14. Relationship between nanowire aspect ratio h/a and fundamental resonant frequency shift f_{scb}/f_{bulk} observed by fixed/free nanowires of constant cross-sectional area, length, and surface area to volume ratio.

Recent atomistic simulations (Liang et al., 2005a; Diao et al., 2006) have indicated that the nanowire elastic properties are strongly dependent upon the amount of compressive surface-stress-driven relaxation strain that the nanowires undergo. We therefore plot in Fig. 15 the variation in nanowire resonant frequencies for the three different geometry types as a function of the percent compressive relaxation strain. As can be observed, while the nanowire resonant frequencies do decrease with increasing relaxation strain, the variation is not the same for the three geometries, which indicates that knowledge of the state of strain is not sufficient to predict the resonant frequencies, and therefore the elastic properties of the fixed/free nanowires. Furthermore, this indicates that the nanowire aspect ratio h/a is the critical geometric parameter for determining the resonant frequency variations due to surface stresses as compared to the corresponding bulk material.

The reduction in resonant frequencies for the fixed/free ⟨1 0 0⟩ nanowires considered in this work is due to the fact that bulk FCC metals tend to soften if compressed in the ⟨1 0 0⟩ direction (Liang et al., 2005a); in the present work, the compression arises due to the surface stresses, rather than any externally applied forces. Therefore, the resonant frequencies for other orientations, for example the ⟨1 1 0⟩ orientation in which FCC metals are known to stiffen under compression (Liang et al., 2005a), may increase rather than decrease for fixed/free boundary conditions as compared to the bulk material.

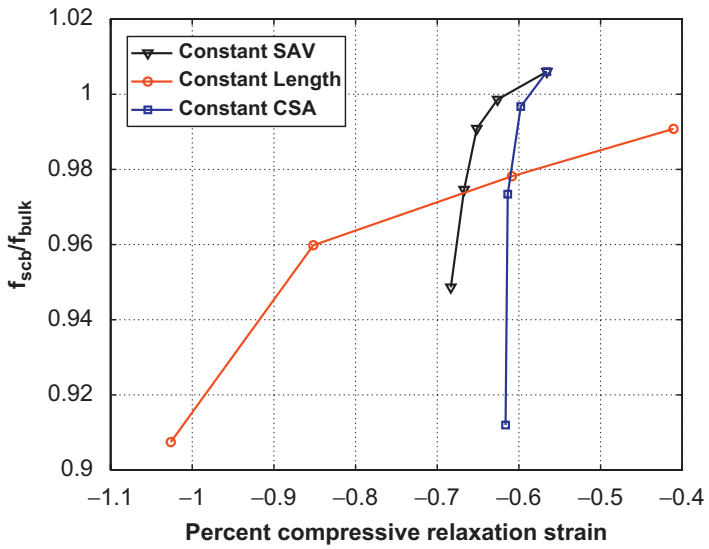

Fig. 15. Relationship between percent compressive relaxation strain and fundamental resonant frequency shift f_{scb}/f_{bulk} observed by fixed/free nanowires of constant cross-sectional area, length, and surface area to volume ratio.

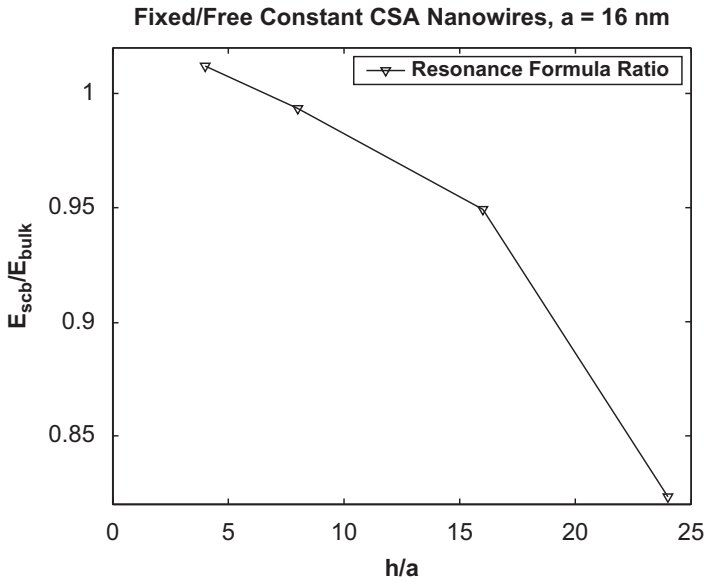

Fig. 16. E_{scb}/E_{bulk} as a function of aspect ratio h/a due to surface stress effects for fixed/free constant CSA nanowires.

We were able to find in the literature one experimental study of free-standing gold nanowires, that of Petrova et al. (2006), who used time-resolved spectroscopy to excite the fundamental resonant mode of ⟨1 0 0⟩ gold nanowires with cross-sectional sizes between 8 and 20 nm. Because the experimentally synthesized wires in that study were free standing, the implication is that the nanowires were also free to relax due to surface stresses. The major result of the Petrova et al. (2006) work is that the resonant frequencies, and thus the elastic properties, were lower than the bulk ⟨1 0 0⟩ modulus for gold, with the postulated reason being due to the elimination of defects in the ultrasmall nanowires.

We note that the SCB calculations in this work, which are also on defect-free nanowires, also predict a decrease in resonant frequency with decreasing nanowire size. We calculated both the SCB and BCB Young's moduli using Eq. (14), with the normalized results for the constant CSA fixed/free nanowires shown in Fig. 16. The present results and the Petrova et al. (2006) results agree in the range of the modulus values; the Petrova et al. (2006) paper reported Young's modulus ranging from about 67% to 93% of the bulk values for nanowire cross-sections ranging from 8 to 18 nm. However, the Petrova work found that the nanowire Young's modulus was independent of SAV ratio, which conflicts with the findings in this work where the nanowire resonant frequencies vary strongly for the same SAV ratio.

In general, we emphasize that the present analysis predicts an increase in resonant frequencies (and thus elastic stiffness) for the fixed/fixed case, while predicting a decrease in resonant frequencies (and thus elastic stiffness) for the fixed/free case. Both of these predictions emerge naturally by correctly obtaining the nanowire state of deformation due to the surface stresses for both fixed/fixed and fixed/free boundary conditions.

4.3. SAV effects

We also discuss the effects of SAV ratio on the predicted nanowire resonant frequencies. To do so, we refer again to the experiments of Verbridge et al. (2006). In that work, an additional key finding was made, in that the fixed/fixed high tensile stress silicon carbide nanostrings were found to have resonant frequencies that did not remain constant for similar SAV ratios. Similarly, no predictive relationship between the variation in the $f_{\text{scb}}/f_{\text{bulk}}$ ratio and SAV ratio could be found for the nanowire geometries considered in this work, which is apparent from studying Figs. 4 and 6, and the constant SAV nanowires in Fig. 7.

Figs. 4 and 6 show opposing trends in the $f_{\text{scb}}/f_{\text{bulk}}$ ratio with increasing SAV ratio, while Fig. 7 shows that for a constant SAV ratio, the $f_{\text{scb}}/f_{\text{bulk}}$ ratio varies with the aspect ratio h/a. Because the resonant frequencies of nanowires appear to be independent of SAV ratio for both large sizes where surface stresses may not be important (Verbridge et al., 2006), and for the current results where surface effects are critical, the implication is that surface stresses are likely to increase the difference between the resonant frequencies of nanowires with the same SAV ratio as that ratio increases with decreasing structural size. These results also correlate with earlier work (Park and Klein, 2007) which showed that the minimum energy configurations of nanowires due to surface stresses are independent of the SAV ratio.

5. Effect of the strain-independent surface stress on the nanowire resonant frequencies

5.1. Motivation and methodology

Traditionally, surface stress has been defined in the mechanics and physics communities as being decomposed into residual (strain-independent) and surface elastic (strain-dependent) parts (Gurtin et al., 1976; Shenoy, 2005; Lu et al., 2005; Cammarata, 1994). This decomposition is typically written as

$$\boldsymbol{\tau}(\boldsymbol{\varepsilon}) = \boldsymbol{\tau}_0 + \mathbf{C}_0\boldsymbol{\varepsilon}, \tag{18}$$

$$\mathbf{C}_0 = \left.\frac{\partial \boldsymbol{\tau}}{\partial \boldsymbol{\varepsilon}}\right|_{\varepsilon=0}, \tag{19}$$

where $\boldsymbol{\tau}_0$ is the residual (strain-independent) part of the surface stress $\boldsymbol{\tau}$, $\mathbf{C}_0\boldsymbol{\varepsilon}$ is the surface elastic (strain-dependent) part of the surface stress, and $\mathbf{C}_0$ is the surface elastic constant, or surface stiffness. Note that Eq. (18) is typically written in terms of the infinitesimal strain $\boldsymbol{\varepsilon}$.

Historically, this decomposition has lead to controversy as to which parts of the surface stress actually alter the resonant frequencies of nanostructures. More than 30 years ago, Gurtin et al. (1976) demonstrated that, within the context of linear elastic continuum beam theory, the resonant frequency is independent of the strain-independent surface stress τ_0. Correspondingly, Lu et al. (2005) recently showed that the resonant frequency of cantilevers is only impacted by the strain-dependent part of the surface stress. However, in contrast, recent work by Lachut and Sader (2007) has also shown that previous analytic models of surface stress effects on the resonant frequencies (McFarland et al., 2005) that are based upon one-dimensional models violate Newton's third law. Lachut and Sader have further noted that the effects of the strain-independent part of the surface stress on the resonant frequencies can only be captured by fully three-dimensional models.

Recently, however, Huang and Wang (2006) and Huang and Sun (2007) considered the effects of the strain-independent surface stress on the elastic properties of nanomaterials within a fully nonlinear, finite deformation context. In doing so, they have conclusively shown that if nanostructure surface effects are studied using fully nonlinear, finite deformation kinematics, there exists a residual surface stress that, unlike the linear case, impacts the overall elastic properties of the nanostructure and which must be accounted for. However, those authors did not consider, within the finite deformation context, the effects of the residual surface stress on the resonant frequencies.

There are significant complexities involved in attempting to separate, due to the large nanowire deformation resulting from the surface stress, the effects of the strain-independent and strain-dependent parts of the surface stress on the resonant frequencies. Due to the nonlinearity, we were not able to exactly separate the strain-independent and strain-dependent parts of the surface stress, for multiple reasons. One reason for this is because if the surface stress is modified to include only the strain-independent part, then by definition, the surface stiffness must also be modified (see Eqs. (10) and (11), or alternatively Eqs. (18) and (19)), as the surface stiffness is the strain derivative of the surface stress. Within the linearized framework that will be utilized in the upcoming discussion that entails removing the strain-dependent surface stiffness $\mathbf{C}_0$ due to the definition in Eq. (19). Furthermore, even if only a strain-independent surface stress is considered, the strain-independent surface stress will cause the nanowire to deform elastically, which causes the bulk stress and stiffness to vary as both are strain-dependent (see Eqs. (8) and (9)). This mechanism of the surface stress causing deformation in the bulk nanowire and thus causing variations in the bulk stress and stiffness was illustrated in the previous numerical examples using the SCB model.

Taking into account the difficulties in delineating the effects of the strain-independent and strain-dependent parts of the surface stress, the approach we take is to modify the surface energy density in Eq. (5) as

$$\gamma(\mathbf{C}) \to \beta(\gamma(\mathbf{C}) - \tfrac{1}{2}\alpha\mathbf{E}^{\mathrm{T}}\tilde{\mathscr{C}}_0\mathbf{E}), \tag{20}$$

where $\mathbf{E} = 0.5(\mathbf{F}^{\mathrm{T}}\mathbf{F} - \mathbf{I})$ is the Green strain tensor, α and β are adjustable parameters, and $\tilde{\mathscr{C}}_0$ is the undeformed surface stiffness, i.e. the surface stiffness defined in Eq. (11) evaluated at $\mathbf{C} = 1$. Taking derivatives of the surface energy in Eq. (20) to get the modified surface stress and surface stiffness, the surface stress that was originally defined in Eq. (10) is modified as

$$\tilde{\mathbf{S}}(\mathbf{C}) \rightarrow \beta\tilde{\mathbf{S}}(\mathbf{C}) - \beta\alpha\tilde{\mathscr{C}}_0\mathbf{E}, \tag{21}$$

while the surface stiffness that was originally defined in Eq. (11) is modified as

$$\tilde{\mathscr{C}}(\mathbf{C}) \rightarrow \beta\tilde{\mathscr{C}}(\mathbf{C}) - \beta\alpha\tilde{\mathscr{C}}_0. \tag{22}$$

The fundamental idea behind the modified surface energy in Eq. (20) leading to the modified surface stress in Eq. (21) and surface stiffness in Eq. (22) is to, in a linearized manner, subtract the contributions from the strain-dependent surface stress and stiffness via the parameters α and β such that the nanowires, upon relaxation to a minimum energy configuration due to surface stresses, will have the same relaxation strain as the results obtained previously using the SCB model, which can be obtained from the above by setting $\alpha = 0$ and $\beta = 1$.

The reason we enforce that the relaxation strain due to surface stresses be the same in the SCB model and the modified SCB model described by Eqs. (20)–(22) is to eliminate any variations in resonant frequency that arise due to the deformation, and therefore the change in stiffness that occurs in the underlying bulk CB material. To find the same relaxation strain using the above modified SCB model as was obtained using the SCB model discussed in earlier sections, we selected $\alpha = 0.5$, then solved for β for each geometry to find the same relaxation strain. The choice of α was also constrained by instabilities in the numerical simulations if the product of α and β exceeded about 0.5; therefore, we chose $\alpha = 0.5$ leading to values of β that ranged from 0.84 to 0.93. We note also that this implies that we were not able to remove the entire contribution of the strain-dependent surface stress. For $\alpha = 0.5$ and varying β, the surface stiffness in Eq. (22) is reduced by approximately 55% as compared to the SCB surface stiffness for both constant CSA and constant length nanowire geometries.

Another reason why we chose α and β such that the modified SCB model in Eqs. (20)–(22) gave the same relaxation strain for a given geometry as the SCB model arises with respect to the SCB surface stress defined in Eq. (10) and the modified surface stress defined in Eq. (21). If the relaxation strain is the same, then the surface stress in Eq. (10) and the modified surface stress in Eq. (21) are equivalent because at the minimum energy configuration at the same relaxed compressive strain, the forces in the bulk material must balance the forces arising due to the surface stress; because the deformation of the bulk is the same, then the surface forces due to the surface stresses that the bulk forces are balancing must also be the same. This can be justified mathematically by differentiating the energy balance in Eq. (1), which leads directly to the bulk and surface force balance just described.

Therefore, the key result of the previous discussion, which is required to interpret the following numerical examples, is that if the SCB surface stress as defined in Eq. (10) and the modified surface stress as defined in Eq. (21) are equivalent at the energy minimum/fully relaxed nanowire configuration, and the bulk deformation is the same, then any difference in resonant frequency between the SCB model and the modified SCB model in Eqs. (20)–(22) arises solely due to differences in the surface stiffness resulting from the subtraction of the strain-dependent part of the surface stress in Eq. (21). Because of this fact, we refer from here on to the modified SCB model described in Eqs. (20)–(22) as the "stiffness modified" SCB model.

5.2. Results and discussion

The comparison between the resonant frequencies calculated earlier using the SCB model ($\alpha = 0$, $\beta = 1$) that was detailed in Section 2.1 and those calculated using the stiffness modified SCB model described in Section 5.1 are shown in Fig. 17 for the fixed/free constant CSA nanowires, and in Fig. 18 for the fixed/fixed constant CSA nanowires.

We pause briefly here to elaborate upon what is being plotted in the figures in this section, taking Fig. 17 as an example. In Fig. 17, we plot both the SCB results obtained using the formulation in Section 2.1, as well as the SCB ($\alpha = 0.5$) results obtained using the stiffness modified SCB formulation in Section 5.1. Because the stiffness modified SCB results are found through subtracting the strain-dependent part of the surface stress and stiffness as shown in Eqs. (21) and (22), the difference between the SCB and SCB ($\alpha = 0.5$) curves represents the resonant frequency shift caused by subtracting the strain-dependent part of the surface stress and stiffness. As discussed earlier, we were not able to subtract the entire contribution of the strain-dependent surface stress, which is why we do not refer to the SCB ($\alpha = 0.5$) curve as the resonant frequency due to the strain-independent surface stress. Therefore, the actual resonant frequencies due to the strain-independent surface stress alone are likely to be further reduced as compared to the SCB ($\alpha = 0.5$) curve in Fig. 17.

One important similarity is that for both fixed/free and fixed/fixed constant CSA nanowires, it is observed that the resonant frequencies calculated using the stiffness modified SCB model are further reduced as compared to the bulk CB resonant frequencies than the SCB resonant frequencies. The lower resonant frequency found using the stiffness modified SCB model occurs, as previously discussed, due to the subtraction of the strain-dependent surface stress in Eq. (21) which results in the reduction of the surface stiffness through Eq. (22).

However, when comparing the results of the stiffness modified SCB resonant frequencies and the SCB resonant frequencies to the bulk value, there are differences that arise depending on the boundary condition. As can be seen for the

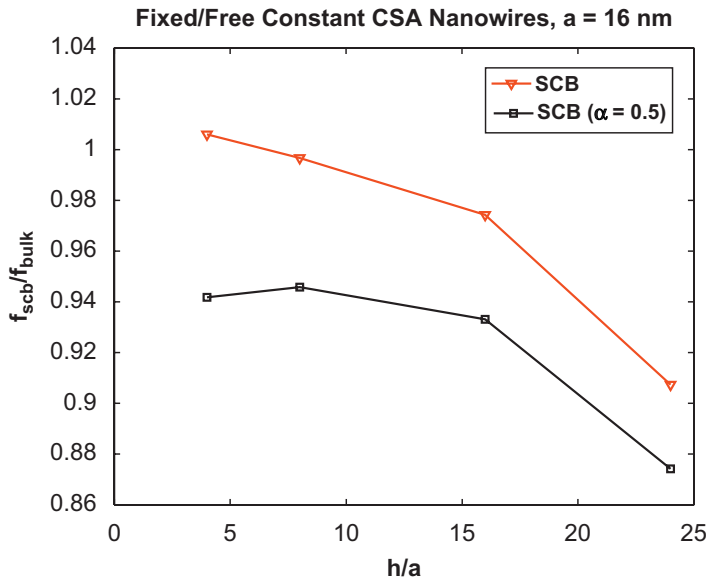

Fig. 17. Effect of subtracting the strain-dependent surface stress and stiffness on the resonant frequencies of fixed/free constant CSA nanowires.

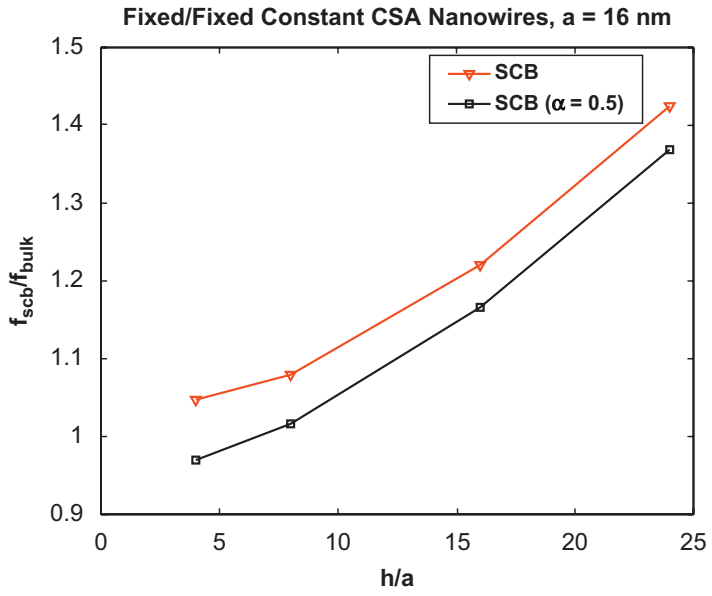

Fig. 18. Effect of subtracting the strain-dependent surface stress and stiffness on the resonant frequencies of fixed/fixed constant CSA nanowires.

fixed/free constant CSA nanowires in Fig. 17, the difference between the stiffness modified SCB and SCB resonant frequencies is larger than the difference between the SCB resonant frequencies and the bulk value until aspect ratios larger than about $h/a = 16$ are reached. Even when $h/a = 24$, the difference between the stiffness modified SCB resonant frequency and the SCB resonant frequency is nearly 4%, which is half of the 8% difference between the SCB resonant frequency and the bulk value; these results strongly indicate that the strain-dependent part of the surface stress has a significant contribution in causing variations in the resonant frequencies of fixed/free constant CSA nanowires as compared to the bulk material.

The opposite trend is observed for the fixed/fixed constant CSA nanowires in Fig. 18; there, the difference between stiffness modified SCB and SCB resonant frequencies as compared to the bulk value is largest at small aspect ratios. As the aspect ratio increases, the difference between the stiffness modified SCB and SCB resonant frequencies is reduced (about 4% when $h/a = 24$) compared to the difference between the SCB resonant frequency and the bulk value, which exceeds 40% when $h/a = 24$.

We also discuss the recent predictions of resonant frequency shift due solely to the strain-independent surface stress by Lachut and Sader (2007). In that work, the following expression was derived for the resonant frequency shift of a fixed/free

beam due to the strain-independent surface stress within the context of linear elastic beam theory:

$$\frac{\Delta\omega}{\omega_0} = -0.042\,\frac{\nu(1-\nu)\sigma_s}{Ew}\left(\frac{b}{h}\right)\left(\frac{b}{w}\right)^2, \tag{23}$$

where $\Delta\omega$ is the shift in resonant frequency, ν is Poisson's ratio, σ_s is the strain-independent surface stress, h is the beam length and w and b are the cross-sectional dimensions. In the present work, the nanowire cross-section is square, i.e. $b = w$, leading to the following simplification of (23):

$$\frac{\Delta\omega}{\omega_0} = -0.042\,\frac{\nu(1-\nu)\sigma_s}{Eh}, \tag{24}$$

which indicates that the shift in resonant frequency due to the strain-independent surface stress should be dependent only on the nanowire length h. To test this hypothesis, we also calculated the variation in resonant frequency using the stiffness modified SCB model for the constant length nanowires, which the Lachut and Sader equation (24) states should be constant if the nanowire length is constant. We note that the SCB results previously shown in this work (see Figs. 5 and 6) clearly indicated a distinct resonant frequency shift due to surface stresses for the constant length case.

The results are shown in Figs. 19 and 20 for the fixed/free and fixed/fixed constant length nanowires, respectively. As can be seen for the fixed/free constant length case in Fig. 19, the change in resonant frequency varies even when the nanowire length is held constant, which disagrees with the analytic expression of Lachut and Sader in Eq. (24). Fig. 20 demonstrates that this is also the case for the fixed/fixed constant length nanowires. Furthermore, the change in resonant frequency is observed to be strongly boundary condition-dependent; fixed/free constant length nanowires show a decrease in resonant frequency with respect to the bulk value with increasing aspect ratio, while fixed/fixed constant length nanowires show an increase in resonant frequency with respect to the bulk value with increasing aspect ratio.

We compare again the resonant frequencies calculated using the stiffness modified SCB model and the SCB model to the bulk value. For the fixed/free constant length nanowires in Fig. 19, the same trend is observed as previously found for the fixed/free constant CSA nanowires in Fig. 17. For the constant length nanowires, the difference between the stiffness modified SCB resonant frequency and the SCB resonant frequency is larger than the difference between the SCB resonant frequency and the bulk value for nearly the entire range of aspect ratios considered. Only when the aspect ratio is large, i.e. $h/a = 24$, is the difference between the stiffness modified SCB and SCB resonant frequency (about 7%) smaller than the difference between the SCB resonant frequency and the bulk value, which is about 9%; this illustrates that the strain-dependent part of the surface stress is significant in shifting the resonant frequencies of fixed/free constant length nanowires as compared to the bulk material.

Furthermore, similar to the fixed/fixed constant CSA nanowires, the fixed/fixed constant length nanowires show an opposite trend, as observed in Fig. 20. There, the difference between stiffness modified SCB and SCB resonant frequencies as compared to the bulk value is largest at small aspect ratios. As the aspect ratio increases, the difference between the stiffness modified SCB and SCB resonant frequencies is reduced (about 6% when $h/a = 24$) compared to the difference between the SCB resonant frequency and the bulk value, which exceeds 60% when $h/a = 24$.

The preceding results collectively demonstrate that the strain-dependent surface stress has a significant effect, one that can be comparable to or even larger than the effect of the strain-independent surface stress depending on the boundary

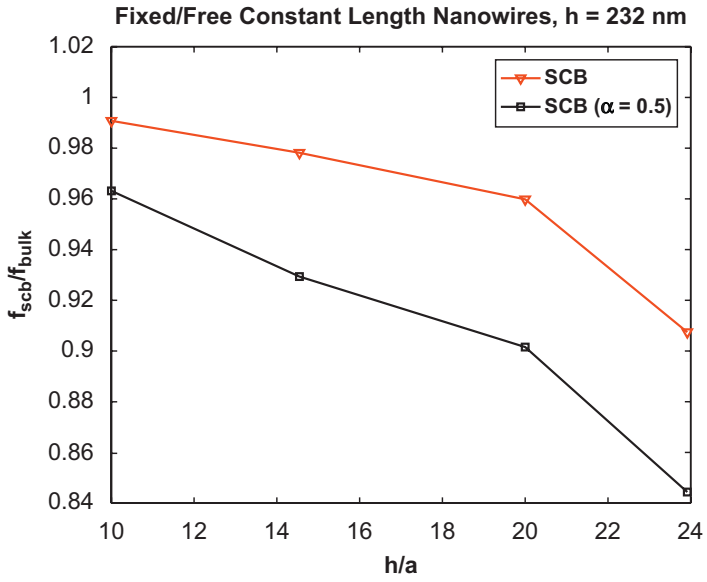

Fig. 19. Effect of subtracting the strain-dependent surface stress and stiffness on the resonant frequencies of fixed/free constant length nanowires.

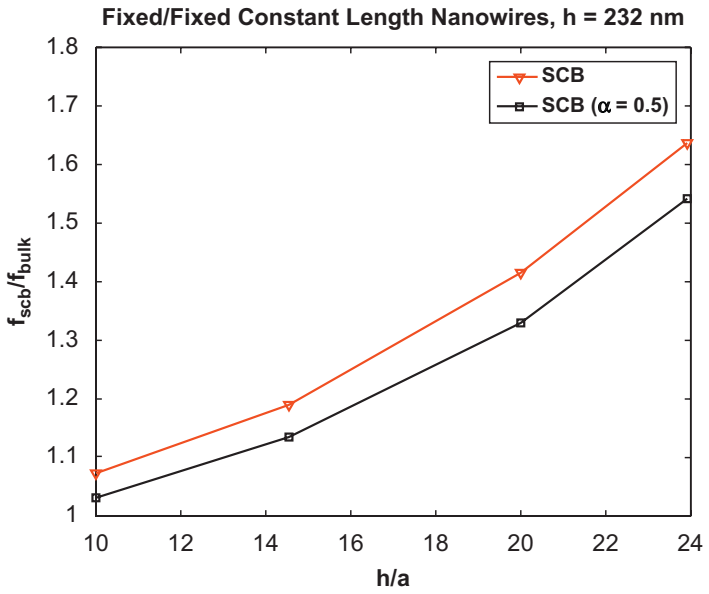

Fig. 20. Effect of subtracting the strain-dependent surface stress and stiffness on the resonant frequencies of fixed/fixed constant length nanowires.

condition, in shifting the resonant frequencies of the nanowires as compared to the bulk material. Furthermore, as discussed earlier, we were not able to remove all effects of the strain-dependent surface stress; removing more of the strain-dependent surface stress would lead to a greater reduction in surface stiffness, leading to even larger deviations in resonant frequency as compared to the bulk material for a given boundary condition.

6. Conclusions

In conclusion, we have utilized the recently developed surface Cauchy–Born model (Park et al., 2006; Park and Klein, 2007, 2008; Park, 2008a, b) to quantify, for the first time, boundary condition and surface stress effects on the resonant properties of fixed/free (cantilevered) and fixed/fixed ⟨1 0 0⟩ gold nanowires with {1 0 0} surfaces. We note that the present analysis was conducted on ideal, non-defective nanowires and thus did not consider factors that are known to deleteriously impact the resonant properties of nanostructures, including clamping losses, internal friction, surface losses and oxidation effects (Ekinci et al., 2004; Cleland and Roukes, 2002; Evoy et al., 1999; Ilic et al., 2004; Yasumura et al., 2000; Carr et al., 1999; Yang et al., 2000; Cuenot et al., 2004; Jing et al., 2006).

Through a parametric study of various nanowire geometries, we draw the following conclusions about surface stress and boundary condition effects on the resonant properties of ⟨1 0 0⟩ gold nanowires with {1 0 0} surfaces: (1) The boundary conditions determine how the nanowires deform in response to the surface stresses. Fixed/free nanowires are able to contract, thus relieving the tensile surface stresses, and leading to an state of compression in the nanowire core that reduces the nanowire resonant frequencies as compared to the bulk material. Fixed/fixed nanowires are constrained such that they cannot deform axially, causing them to exist in a state of tensile stress, and elevating their resonant frequencies as compared to the bulk material. (2) The reduction in resonant frequencies for the fixed/free boundary condition and increase in resonant frequencies for the fixed/fixed boundary condition indicate that those nanowires are expected to be elastically softer, and stiffer, respectively, than the corresponding bulk material, agreeing with recent experimental results for both free-standing (Petrova et al., 2006), and fixed/fixed nanowires (Cuenot et al., 2004; Jing et al., 2006; Husain et al., 2003). (3) The variation in nanowire resonant frequencies due to surface stresses for the various geometries was found to be dependent on a geometric factor, the nanowire aspect ratio h/a. In contrast, no dependence of the resonant frequencies on the SAV ratio was found, again agreeing with recent experimental data (Verbridge et al., 2006; Petrova et al., 2006). (4) The variation in resonant frequency for the fixed/free case occurs due to the fact the bulk ⟨1 0 0⟩ material softens under compression. Because of this, the resonant frequencies of fixed/free nanowires of other orientations that stiffen under compression, such as ⟨1 1 0⟩, are expected to increase rather than decrease as compared to the corresponding bulk material. (5) In analyzing the higher order resonant modes (second bending, stretch, twist), surface stresses cause the largest variation in the second bending frequencies, while the twist and stretch frequencies show little variation due to surface stresses. (6) All higher order resonant frequencies decrease with respect to the fundamental bending frequency with increasing aspect ratio for fixed/fixed nanowires due to surface stresses, while the opposite is true, i.e. the higher order resonant frequencies increase with respect to the fundamental bending frequency for fixed/free nanowires.

We have also, for the first time, quantified the effects of both the residual (strain-independent) and surface elastic (strain-dependent) parts of the surface stress on the resonant frequencies of metal nanowires if fully nonlinear, finite

deformation kinematics are utilized. We find that if finite deformation kinematics are considered, the strain-independent surface stress substantially alters the resonant frequencies of the nanowires. However, we also find that the strain-dependent surface stress has a significant effect, one that can be comparable to or even larger than the effect of the strain-independent surface stress depending on the boundary condition, in shifting the resonant frequencies of the nanowires as compared to the bulk material. In particular, we found, using the stiffness modified SCB model described in Section 5.1 that: (1) Fixed/free nanowires, due to their state of compression resulting from the surface stresses, show resonant frequencies that are considerably reduced as compared to a standard bulk continuum model. Furthermore, it is for the fixed/free nanowires that the strain-dependent surface stress is found to have the largest effect on the resonant frequencies, with the effect being comparable to or even larger than the effect of the strain-independent surface stress in shifting the resonant frequencies of fixed/free nanowires as compared to the bulk material. (2) Fixed/fixed nanowires, due to the state of tensile stress resulting from the fixed end boundary conditions and the tensile nature of the surface stress, show resonant frequencies that are considerably elevated as compared to the standard bulk continuum model. It was determined that the strain-dependent surface stress had a much smaller effect on fixed/fixed nanowires, with the largest impact made at smaller aspect ratios.

A key point to highlight with regards to the preceding discussion is that because the surface stiffness does contribute to the observed resonant frequency variation, it cannot be set arbitrarily. This point was gleaned through utilization of the stiffness modified SCB model in Section 5.1 to obtain the same compressive relaxation due to surface stresses as the SCB model. Despite the equivalence in the state of deformation, which was imposed so as to eliminate any effects on the resonant frequency that could occur due to variations in the bulk stiffness arising from different states of deformation, the resonant frequency predictions were significantly different, which indicates that knowledge of the amount of strain in the nanowire after deformation due to surface stresses is not sufficient to predict the resulting resonant frequencies. This point is also illustrated in Figs. 14 and 15, which show the variation in resonant frequency for the fixed/free nanowires using the SCB model depended on the nanowire aspect ratio, and not the amount of compressive relaxation strain the nanowire free end undergoes due to surface stresses. The SCB model developed in the present work thus has the distinct advantage that the surface stiffness is derived directly from the underlying lattice structure and interatomic potential, which is preferable to phenomenological approaches to deriving a surface elastic constitutive model.

We close by discussing the implications of the present work with regards to the standard linear elastic beam theories that are often utilized to interpret the elastic properties of nanowires. The results we have obtained have shown in all cases that the elastic properties of nanowires, when surface stress effects are fully accounted for using nonlinear, finite deformation kinematics, show substantial deviations from those predicted by linear elastic continuum beam theory. This fact is evident in the resonant frequencies predicted using the SCB model for both fixed/free and fixed/fixed boundary conditions, and were further evident in comparing results obtained in the present work to those for the resonant frequencies of (linear elastic) beams when both the strain-independent and strain-dependent parts of the surface stress were considered. Considering the large, nonlinear deformations that metal nanowires are known to undergo due to surface stresses in which the nanowire compressive strain can easily exceed 0.5% (Diao et al., 2003; Park et al., 2005; Park and Klein, 2007), it is clear that nonlinear, finite deformation kinematics should be utilized in describing the deformation, and thus the elastic properties of nanowires, when surface stress effects are significant.

Acknowledgments

H.S.P. gratefully acknowledges NSF Grant no. CMMI-0750395 in support of this research. Both authors gratefully acknowledge the assistance of Heidi Thorn, Michael Heroux, Roscoe Bartlett and the Sandia Trilinos team in support of this research. H.S.P. also acknowledges helpful discussions with Prof. Y.-C. Chen on the resonant frequency calculations. Both authors acknowledge the reviewers for their insightful comments.

References

Balamane, H., Halicioglu, T., Tiller, W.A., 1992. Comparative study of silicon empirical interatomic potentials. Phys. Rev. B 46 (4), 2250–2279.
Barnes, W.L., Dereux, A., Ebbeson, T.W., 2003. Surface plasmon subwavelength optics. Nature 424, 824–830.
Belytschko, T., Liu, W.K., Moran, B., 2002. Nonlinear Finite Elements for Continua and Structures. Wiley, New York.
Cammarata, R.C., 1994. Surface and interface stress effects in thin films. Progr. Surf. Sci. 46 (1), 1–38.
Canham, L.T., 1990. Silicon quantum wire array fabricated by electrochemical and chemical dissolution of wafers. Appl. Phys. Lett. 57 (10), 1046–1048.
Carr, D.W., Evoy, S., Sekaric, L., Craighead, H.G., Parpia, J.M., 1999. Measurement of mechanical resonance and losses in nanometer scale silicon wires. Appl. Phys. Lett. 75 (7), 920–922.
Chen, Y., Dorgan, B.L., McIlroy, D.N., Aston, D.E., 2006. On the importance of boundary conditions on nanomechanical bending behavior and elastic modulus determination of silver nanowires. J. Appl. Phys. 100, 104301.
Cleland, A.N., Roukes, M.L., 1996. Fabrication of high frequency nanometer scale mechanical resonators from bulk Si crystals. Appl. Phys. Lett. 69 (18), 2653–2655.
Cleland, A.N., Roukes, M.L., 2002. Noise processes in nanomechanical resonators. J. Appl. Phys. 92 (5), 2758–2769.
Craighead, H.G., 2000. Nanoelectromechanical systems. Science 290, 1532–1535.
Cuenot, S., Frétigny, C., Demoustier-Champagne, S., Nysten, B., 2004. Surface tension effect on the mechanical properties of nanomaterials measured by atomic force microscopy. Phys. Rev. B 69, 165410.
Davis, Z.J., Boisen, A., 2005. Aluminum nanocantilevers for high sensitivity mass sensors. Appl. Phys. Lett. 87, 013102.

Daw, M.S., Baskes, M.I., 1984. Embedded-atom method: derivation and application to impurities, surfaces, and other defects in metals. Phys. Rev. B 29 (12), 6443–6453.
Diao, J., Gall, K., Dunn, M.L., 2003. Surface-stress-induced phase transformation in metal nanowires. Nat. Mater. 2 (10), 656–660.
Diao, J., Gall, K., Dunn, M.L., Zimmerman, J.A., 2006. Atomistic simulations of the yielding of gold nanowires. Acta Mater. 54, 643–653.
Dikin, D.A., Chen, X., Ding, W., Wagner, G., Ruoff, R.S., 2003. Resonance vibration of amorphous SiO_2 nanowires driven by mechanical or electrical field excitation. J. Appl. Phys. 93 (1), 226–230.
Dingreville, R., Qu, J., Cherkaoui, M., 2005. Surface free energy and its effect on the elastic behavior of nano-sized particles, wires and films. J. Mech. Phys. Solids 53, 1827–1854.
Ekinci, K.L., 2005. Electromechanical transducers at the nanoscale: actuation and sensing of motion in nanoelectromechanical systems (NEMS). Small 1 (8–9), 786–797.
Ekinci, K.L., Roukes, M.L., 2005. Nanoelectromechanical systems. Rev. Sci. Instrum. 76, 061101.
Ekinci, K.L., Yang, Y.T., Roukes, M.L., 2004. Ultimate limits to inertial mass sensing based upon nanoelectromechanical systems. J. Appl. Phys. 95 (5), 2682–2689.
Evoy, S., Carr, D.W., Sekaric, L., Olkhovets, A., Parpia, J.M., Craighead, H.G., 1999. Nanofabrication and electrostatic operation of single-crystal silicon paddle oscillators. J. Appl. Phys. 86 (11), 6072–6077.
Evoy, S., Olkhovets, A., Sekaric, L., Parpia, J.M., Craighead, H.G., Carr, D.W., 2000. Temperature-dependent internal friction in silicon nanoelectromechanical systems. Appl. Phys. Lett. 77 (15), 2397–2399.
Foiles, S.M., Baskes, M.I., Daw, M.S., 1986. Embedded-atom-method functions for the FCC metals Cu, Ag, Au, Ni, Pd, Pt, and their alloys. Phys. Rev. B 33 (12), 7893–7991.
Gurtin, M.E., Murdoch, A., 1975. A continuum theory of elastic material surfaces. Arch. Ration. Mech. Anal. 57, 291–323.
Gurtin, M.E., Markenscoff, X., Thurston, R.N., 1976. Effects of surface stress on the natural frequency of thin crystals. Appl. Phys. Lett. 29 (9), 529–530.
Haiss, W., 2001. Surface stress of clean and adsorbate-covered solids. Rep. Progr. Phys. 64, 591–648.
Hasmy, A., Medina, E., 2002. Thickness induced structural transition in suspended FCC metal nanofilms. Phys. Rev. Lett. 88 (9), 096103.
Heidelberg, A., Ngo, L.T., Wu, B., Phillips, M.A., Sharma, S., Kamins, T.I., Sader, J.E., Boland, J.J., 2006. A generalized description of the elastic properties of nanowires. Nano Lett. 6 (6), 1101–1106.
Hoffmann, S., Utke, I., Moser, B., Michler, J., Christiansen, S.H., Schmidt, V., Senz, S., Werner, P., Gosele, U., Ballif, C., 2006. Measurement of the bending strength of vapor–liquid–solid grown silicon nanowires. Nano Lett. 6 (4), 622–625.
Houston, B.H., Photiadis, D.M., Marcus, M.H., Bucaro, J.A., Liu, X., Vignola, J.F., 1976. Thermoelastic loss in microscale oscillators. Appl. Phys. Lett. 80 (7), 1300–1302.
Huang, Z.P., Sun, L., 2007. Size-dependent effective properties of a heterogeneous material with interface energy effect: from finite deformation theory to infinitesimal strain analysis. Acta Mech. 190, 151–163.
Huang, Z.P., Wang, J., 2006. A theory of hyperelasticity of multi-phase media with surface/interface energy effect. Acta Mech. 182, 195–210.
Huang, G.Y., Gao, W., Yu, S.W., 2006. Model for the adsorption-induced change in resonance frequency of a cantilever. Appl. Phys. Lett. 89, 043506.
Huang, X.M.H., Zorman, C.A., Mehregany, M., Roukes, M.L., 2003. Nanodevice motion at microwave frequencies. Nature 42, 496.
Husain, A., Hone, J., Postma, H.W.C., Huang, X.M.H., Drake, T., Barbic, M., Scherer, A., Roukes, M.L., 2003. Nanowire-based very-high-frequency electromechanical oscillator. Appl. Phys. Lett. 83 (6), 1240–1242.
Ilic, B., Craighead, H.G., Krylov, S., Senaratne, W., Ober, C., Neuzil, P., 2004. Attogram detection using nanoelectromechanical oscillators. J. Appl. Phys. 95 (7), 3694–3703.
Jing, G.Y., Duan, H.L., Sun, X.M., Zhang, Z.S., Xu, J., Li, Y.D., Wang, J.X., Yu, D.P., 2006. Surface effects on elastic properties of silver nanowires: contact atomic-force microscopy. Phys. Rev. B 73, 235409.
Kondo, Y., Ru, Q., Takayanagi, K., 1999. Thickness induced structural phase transition of gold nanofilm. Phys. Rev. Lett. 82 (4), 751–754.
Lachut, M.J., Sader, J.E., 2007. Effect of surface stress on the stiffness of cantilever plates. Phys. Rev. Lett. 99, 206102.
Lavrik, N.V., Sepaniak, M.J., Datskos, P.G., 2004. Cantilever transducers as a platform for chemical and biological sensors. Rev. Sci. Instrum. 75 (7), 2229–2253.
Li, D., Wu, Y., Kim, P., Shi, L., Yang, P., Majumdar, A., 2003. Thermal conductivity of individual silicon nanowires. Appl. Phys. Lett. 83 (14), 2934–2936.
Li, M., Mayer, T.S., Sioss, J.A., Keating, C.D., Bhiladvala, R.B., 2007. Template-grown metal nanowires as resonators: performance and characterization of dissipative and elastic properties. Nano Lett. 7 (11), 3281–3284.
Li, X., Ono, T., Wang, Y., Esashi, M., 2003. Ultrathin single-crystalline-silicon cantilever resonators: fabrication technology and significant specimen size effect on Young's modulus. Appl. Phys. Lett. 83 (15), 3081–3083.
Liang, H., Upmanyu, M., Huang, H., 2005a. Size-dependent elasticity of nanowires: nonlinear effects. Phys. Rev. B 71, 241403(R).
Liang, W., Zhou, M., Ke, F., 2005b. Shape memory effect in Cu nanowires. Nano Lett. 5 (10), 2039–2043.
Lieber, C.M., 2003. Nanoscale science and technology: building a big future from small things. MRS Bull. 28 (7), 486–491.
Lu, P., Lee, H.P., Lu, C., O'Shea, S.J., 2005. Surface stress effects on the resonance properties of cantilever sensors. Phys. Rev. B 72, 085405.
McFarland, A.W., Poggi, M.A., Doyle, M.J., Bottomley, L.A., Colton, J.S., 2005. Influence of surface stress on the resonance behavior of microcantilevers. Appl. Phys. Lett. 87, 053505.
Miller, R.E., Shenoy, V.B., 2000. Size-dependent elastic properties of nanosized structural elements. Nanotechnology 11, 139–147.
Nam, C.Y., Jaroenapibal, P., Tham, D., Luzzi, D.E., Evoy, S., Fischer, J.E., 2006. Diameter-dependent electromechanical properties of GaN nanowires. Nano Lett. 6 (2), 153–158.
Namazu, T., Isono, Y., Tanaka, T., 2000. Evaluation of size effect on mechanical properties of single crystal silicon by nanoscale bending test using AFM. J. Microelectromechanical Syst. 9 (4), 450–459.
Ohnishi, H., Kondo, Y., Takayanagi, K., 1998. Quantized conductance through individual rows of suspended gold atoms. Nature 395, 780–783.
Park, H.S., 2008a. Strain sensing through the resonant properties of deformed metal nanowires. J. Appl. Phys. 104, 013516.
Park, H.S., 2008b. Surface stress effects on the resonant properties of silicon nanowires. J. Appl. Phys. 103, 123504.
Park, H.S., Klein, P.A., 2007. Surface Cauchy–Born analysis of surface stress effects on metallic nanowires. Phys. Rev. B 75, 085408.
Park, H.S., Klein, P.A., 2008. A surface Cauchy–Born model for silicon nanostructures. Comput. Methods Appl. Mech. Eng. 197, 3249–3260.
Park, H.S., Gall, K., Zimmerman, J.A., 2005. Shape memory and pseudoelasticity in metal nanowires. Phys. Rev. Lett. 95, 255504.
Park, H.S., Klein, P.A., Wagner, G.J., 2006. A surface Cauchy–Born model for nanoscale materials. Int. J. Numer. Methods Eng. 68, 1072–1095.
Petrova, H., Perez-Juste, J., Zhang, Z.Y., Zhang, J., Kosel, T., Hartland, G.V., 2006. Crystal structure dependence of the elastic constants of gold nanorods. J. Mater. Chem. 16 (40), 3957–3963.
Rubio, G., Agrait, N., Vieira, S., 1996. Atomic-sized metallic contacts: mechanical properties and electronic transport. Phys. Rev. Lett. 76 (13), 2302–2305.
Sader, J.E., 2001. Surface stress induced deflections of cantilever plates with applications to the atomic force microscope: rectangular plates. J. Appl. Phys. 89 (5), 2911–2921.
Sharma, P., Ganti, S., Bhate, N., 2003. Effect of surfaces on the size-dependent elastic state of nano-inhomogeneities. Appl. Phys. Lett. 82 (4), 535–537.
Shenoy, V.B., 2005. Atomistic calculations of elastic properties of metallic FCC crystal surfaces. Phys. Rev. B 71, 094104.
Sun, C.T., Zhang, H., 2003. Size-dependent elastic moduli of platelike nanomaterials. J. Appl. Phys. 92 (2), 1212–1218.
Sundararajan, S., Bhushan, B., Namazu, T., Isono, Y., 2002. Mechanical property measurements of nanoscale structures using an atomic force microscope. Ultramicroscopy 91, 111–118.
Tadmor, E., Ortiz, M., Phillips, R., 1996. Quasicontinuum analysis of defects in solids. Philos. Mag. A 73, 1529–1563.
Tahoe, ⟨http://tahoe.ca.sandia.gov⟩.

Tang, Z., Zhao, H., Li, G., Aluru, N.R., 2006. Finite-temperature quasicontinuum method for multiscale analysis of silicon nanostructures. Phys. Rev. B 74, 064110.
Trilinos, ⟨http://software.sandia.gov/trilinos/index.html⟩.
Verbridge, S.S., Parpia, J.M., Reichenbach, R.B., Bellan, L.M., Craighead, H.G., 2006. High quality factor resonance at room temperature with nanostrings under high tensile stress. J. Appl. Phys. 99, 124304.
Verbridge, S.S., Shapiro, D.F., Craighead, H.G., Parpia, J.M., 2007. Macroscopic tuning of nanomechanics: substrate bending for reversible control of frequency and quality factor of nanostring resonators. Nano Lett. 7 (6), 1728–1735.
Wan, J., Fan, Y.L., Gong, D.W., Shen, S.G., Fan, X.Q., 1999. Surface relaxation and stress of FCC metals: Cu, Ag, Au, Ni, Pd, Pt, Al and Pb. Modelling Simulation Mater. Sci. Eng. 7, 189–206.
Wang, J., Duan, H.L., Huang, Z.P., Karihaloo, B.L., 2006. A scaling law for properties of nano-structured materials. Proc. R. Soc. A 462, 1355–1363.
Weaver, W., Timoshenko, S.P., Young, D.H., 1990. Vibration Problems in Engineering. Wiley, New York.
Wei, G., Shouwen, Y., Ganyun, H., 2006. Finite element characterization of the size-dependent mechanical behaviour in nanosystems. Nanotechnology 17, 1118–1122.
Wiley, B.J., Wang, Z., Wei, J., Yin, Y., Cobden, D.H., Xia, Y., 2006. Synthesis and electrical characterization of silver nanobeams. Nano Lett. 6 (10), 2273–2278.
Wong, E.W., Sheehan, P.E., Lieber, C.M., 1997. Nanobeam mechanics: elasticity, strength, and toughness of nanorods and nanotubes. Science 277, 1971–1975.
Wu, B., Heidelberg, A., Boland, J.J., 2005. Mechanical properties of ultrahigh-strength gold nanowires. Nat. Mater. 4, 525–529.
Xia, Y., Yang, P., Sun, Y., Wu, Y., Mayers, B., Gates, B., Yin, Y., Kim, F., Yan, H., 2003. One-dimensional nanostructures: synthesis, characterization, and applications. Adv. Mater. 15 (5), 353–389.
Yang, J., Ono, T., Esashi, M., 2000. Surface effects and high quality factors in ultrathin single-crystal silicon cantilevers. Appl. Phys. Lett. 77 (23), 3860–3862.
Yang, J., Ono, T., Esashi, M., 2001. Investigating surface stress: surface loss in ultrathin single-crystal silicon cantilevers. J. Vac. Sci. Technol. B 19 (2), 551–556.
Yasumura, K.Y., Stowe, T.D., Chow, E.M., Pfafman, T., Kenny, T.W., Stipe, B.C., Rugar, D., 2000. Quality factors in micron- and submicron-thick cantilevers. J. Microelectromechanical Syst. 9 (1), 117–125.
Zhou, L.G., Huang, H., 2004. Are surfaces elastically softer or stiffer? Appl. Phys. Lett. 84 (11), 1940–1942.